REPORT DOCUMENTATION PAGE

Form Approved
OMB No. 0704-0188

The public reporting burden for this collection of information is estimated to average 1 hour per response, including the time for reviewing instructions, searching existing data sources, gathering and maintaining the data needed, and completing and reviewing the collection of information. Send comments regarding this burden estimate or any other aspect of this collection of information, including suggestions for reducing the burden, to Department of Defense, Washington Headquarters Services, Directorate for Information Operations and Reports (0704-0188), 1215 Jefferson Davis Highway, Suite 1204, Arlington, VA 22202-4302. Respondents should be aware that notwithstanding any other provision of law, no person shall be subject to any penalty for failing to comply with a collection of information if it does not display a currently valid OMB control number.
PLEASE DO NOT RETURN YOUR FORM TO THE ABOVE ADDRESS.

1. REPORT DATE *(DD-MM-YYYY)*
31/07/2008

2. REPORT TYPE
Final Report

3. DATES COVERED *(From - To)*
April 2004 - May 2008

4. TITLE AND SUBTITLE
Power Packaging of Spray-Cooled SiC Devices for High Temperature and High Voltage Operation: Final Report

5a. CONTRACT NUMBER

5b. GRANT NUMBER
N00014-04-1-0603

5c. PROGRAM ELEMENT NUMBER

5d. PROJECT NUMBER
07PR05674-00

5e. TASK NUMBER

5f. WORK UNIT NUMBER

6. AUTHOR(S)
Juan Carlos Balda, R. Panneer Selvam, Brian Rowden

7. PERFORMING ORGANIZATION NAME(S) AND ADDRESS(ES)
University of Arkansas
Office of Contracts and Grants
Fayetteville, AR 72701

8. PERFORMING ORGANIZATION REPORT NUMBER
FR1

9. SPONSORING/MONITORING AGENCY NAME(S) AND ADDRESS(ES)
Office of Naval Research
875 North Randolph Street
Arlington, VA 22203-1995

10. SPONSOR/MONITOR'S ACRONYM(S)
ONR 331

11. SPONSOR/MONITOR'S REPORT NUMBER(S)

12. DISTRIBUTION/AVAILABILITY STATEMENT
Approved for Public Release, distribution is Unlimited

13. SUPPLEMENTARY NOTES

14. ABSTRACT
Main objective was developing the foundation for designing sprayed-cooled power packages for semiconductors like silicon-carbide devices capable of high temperature and voltage operation. Research addressed: (1) Understanding of the heat transfer phenomenon during spray cooling under phase change; (2) Packaging materials for high temperature and spray cooling or jet impingement; (3) A scaled-down spray-cooled power package of a power conversion module; and (4) New electric topologies of power conversion modules for integration with spray-cooling solutions. Main conclusions were: (a) Quick replacement of hot liquid by cold liquid (i.e., transient conduction) is main mechanism enabling high heat fluxes; (b) Jet impingement without nozzles provides cost effective solutions; (c) Several high temperature active metal brazing materials suitable for high temperature die attach but requiring more research to ensure proper chemical behavior; (d) A double-sided power package providing minimized volumetric footprint for the spray box and integrates the power electronic systems; and (e) Several new electric topologies of power conversion modules.

15. SUBJECT TERMS
spray cooling thermal solution, power packaging, high temperature die attach, power conversion modules, double-sided spray cooling

16. SECURITY CLASSIFICATION OF:			17. LIMITATION OF ABSTRACT	18. NUMBER OF PAGES	19a. NAME OF RESPONSIBLE PERSON
a. REPORT	b. ABSTRACT	c. THIS PAGE			Juan Carlos Balda
U	U	U	UU	54	19b. TELEPHONE NUMBER (Include area code) 479-575-3005

POWER PACKAGING OF SPRAY-COOLED SiC DEVICES FOR HIGH TEMPERATURE AND HIGH VOLTAGE OPERATION: FINAL REPORT

Award. N00014-04-1-0603

Period of Performance: April 01, 2004 – May 31, 2008

Final Report (FR1)

Juan Carlos Balda, R. Panneer Selvam, Brian Rowden

University of Arkansas
Department of Electrical Engineering
3217 Bell Engineering Center
Fayetteville, AR 72701–1201
(479) 575-3005

Prepared for

Office of Naval Research 331
875 North Randolph Street
Arlington, VA 22203-1995

July 2008

20080811 050

Contract Information

Contract Number	N00014-04-1-0603
Title of Research	POWER PACKAGING OF SPRAY-COOLED SiC DEVICES FOR HIGH TEMPERATURE AND HIGH VOLTAGE OPERATION
Principal Investigator	Juan Carlos Balda
Organization	University of Arkansas, Fayetteville

Technical Section

Technical Objectives

The main objective of this project was to develop the technical foundation for the design and fabrication of power packages based on spray cooling for semiconductor devices like silicon-carbide (SiC) power devices which are capable of operating at high temperatures and high voltages. This objective was accomplished through the following enabling objectives:

(1) Developing a mathematical understanding of the heat transfer phenomenon during liquid spray cooling under phase change in order to facilitate the design of spray-cooled power modules.

(2) Analyzing packaging materials for SiC devices that can operate at high temperatures, greater than 200 °C, and are compatible with spray cooling.

(3) Demonstrating the feasibility of a spray-cooled power package on a scaled-down prototype of a power conversion module (PCM).

(4) Developing new electric topologies of power conversion modules suitable for integration with spray-cooling thermal solutions.

The above enabling objectives set by the multi-disciplinary research group at the University of Arkansas (UA) addressed issues related to power conversion modules (PCM) for electric ships that are normally addressed by two different research groups. The thermal management group normally evaluates the heat-transfer issues while power-electronic group normally evaluates the electric power conversion issues. These two constituencies are often at different organizations or different research groups within the same organization with little interaction between each other. So, a third group (or additional contract phase) is often needed to optimize the entire system leading to longer developmental times.

Technical Approach

Bearing in mind the above enabling objectives, the project activities were initially divided into the following main tasks:

- Task 1: Organizational Meeting
- Task 2: Mathematical Modeling of Spray Phenomenon for System Design Purposes
    - Sub-task 2.1: Computer Modeling of Spray Cooling
    - Sub-task 2.2: Experimental Results Using Spray Cooling
    - Sub-task 2.3: Experimental Results Using Liquid Jet
- Task 3: Development of Spray-Cooled Power Modules
    - Sub-task 3.1: Packaging of SiC Diodes
    - Sub-task 3.2: Investigation of High-Temperature Die Attach Materials

- Sub-task 3.3: Packaging of Spray-Cooled Power Conversion Modules

- Task 4: Technology Demonstrator
  - Sub-task 4.1: Multi-level Converters
  - Sub-task 4.2: Novel Topologies for Interfacing Multiple Non-Traditional Sources to an ac Power Grid
- Task 5: Recommendations for Future Research Work

Bearing in mind the multi-disciplinary nature of the reported research activities, each sub-task has been written in such a manner that they stand alone for most cases (for example, a reader interested on thermal management issues should identify the report contributions in this field by reading only those thermal management sections). References are included with each task and the publications produced by the research work on this ONR grant are given at the end of this report.

For those readers interested the work performed and completed on the final year of this ONR grant, the associated research activities are addressed in the following sub-tasks:

- Sub-task 2.2: Experimental Results Using Spray Cooling
- Sub-task 2.3: Experimental Results Using Liquid Jet
- Sub-task 3.3: Spray-Cooled Power Conversion Modules
- Sub-task 4.2: Novel Topologies for Interfacing Multiple Non-Traditional Sources to an ac Power Grid

Project Final Report

This Final Report summarizes the activities performed on this grant from its beginning on April 1, 2004, through its conclusion on May 31, 2008. The faculty research team consisted of Drs. J. C. Balda, R. P. Selvam, Dr. F. D. Barlow and Dr. A. Elshabini. On July 2006, Drs. F. D. Barlow and A. Elshabini moved to the University of Idaho. Graduate students who worked on this project were:

- Mita Sarkar (doctoral student who graduated in July 2008),
- Brian Rowden (doctoral student anticipating his graduation in fall 2008),
- Kiran Vanam (doctoral student anticipating his graduation in fall 2008 and currently working for Texas Instruments in Dallas, TX),
- Joe Carr (doctoral student anticipating his graduation in summer 2009),
- Ananta Medury (master student who graduated in February 2007 and now is working for Northrop Grumman in Baltimore),
- Ranadheer Purupati (master student)

Specific activities performed under the grant tasks are described below.

Task 2: Computer Modeling for Spray Cooling

The technical leader of this task is Dr. R. Panneer Selvam who was helped by Mrs. Mita Sarkar who completed her doctoral studies in July 2008.

The activities performed under this task could be divided into three sub-tasks; namely

- Sub-task 2.1: Computer Modeling of Spray Cooling
- Sub-task 2.2: Experimental Results Using Spray Cooling
- Sub-task 2.3: Experimental Results Using Liquid Jet

Sub-task 2.1: Computer Modeling of Spray Cooling

Spray cooling is a way of efficiently removing the heat from a surface and considered for high power systems such as advanced lasers. Spray cooling with phase change and droplet impact can achieve heat fluxes up to 1000 W/cm^2 as reported by Yang et al. [2.1]. Several experiments have been conducted using spray cooling in recent years [2.2-2.5] and designs of spray cooling devices are emerging. Theoretical understanding of the spray-cooling heat-acquisition phenomena is still in its infancy and focused efforts to develop a comprehensive numerical model like those in this ONR grant are of prime importance to this field.

Selvam [2.7] and Selvam et al. [2.8] identified that computer modeling of nucleation boiling in a thin film in the neighborhood of 70-μm deep provides valuable information for designing experiments for spray cooling. A survey on the current status of computational modeling of spray cooling was presented and details of methods to solve multiphase flow were reported. Preliminary computation of growing a vapor bubble in a thin film of liquid and the transient heat transfer on the wall were reported. They identified that high heat transfer takes place during the impact of liquid droplet on the thin liquid film where vapor bubble is growing. Selvam et al. [2.6] concluded from their study that when the vapor bubble grows on a hot wall, the heat transfer from the wall gets reduced. Therefore, the vapor bubble growth and movement from the wall were investigated to evaluate the effect on heat transfer rate.

Recently, Selvam et al. [2.8-2.9] worked on computer modeling of droplet impact on vapor bubble growth in thin film of liquid. This work considered both vapor and liquid in the computational region. They identified that the collapse of the vapor bubble in the liquid layer by liquid droplet impacting at high speed and the vapor bubble breaking during the merging of vapor on the top of the thin liquid film had major impacts on spray cooling heat transfer. They also identified that the effect of the density ratio on heat transfer was not significant.

Further work on computer modeling of droplet impact on vapor bubble growth in thin film of liquid is reported in [2.10-2.13]. These works considered both vapor and liquid in the computational region. In these studies the computer model was used to investigate the spray cooling phenomenon in the micro environment of about 44 μm thickness liquid layers with vapor bubble growing due to nucleation and droplet impact. Using the model the effect of vapor bubble size, thermal conductivity and latent heat of vaporization of liquid on heat flux was investigated. Reference [2.13] provides a detail discussion of model development and some of the investigations; this information is not included in this report because of simplicity, ease of reading and space.

Conclusions

From the researcher's studies the following conclusions are made:

1. The level set method was selected for numerical modeling of multiphase flow in spray cooling using. The model considered the effect of surface tension between liquid and vapor, gravity, phase change and viscosity. The computer model was used to study the spray cooling phenomenon in the micro environment of about 44-μm thickness liquid layers with vapor bubble

growing due to nucleation. The importance of studying the heat transfer mechanism in a thin liquid film for spray cooling was identified. The flow and heat transfer details were presented when a liquid droplet impacted the thin liquid layer with a growing vapor bubble.

2. For high heat-flux spray cooling, the thin film on the heated surface and its interaction with liquid droplet were very important.
3. It was observed that the maximum heat flux obtained in terms of the Nusselt number Nu increases with increased vapor bubble size and the maximum Nu is reached in a shorter time for the bubble radius of 0.05 units (36.8 μm) compared to smaller bubble radius.
4. The heat flux increases with increasing thermal conductivity of the liquid. Overall increase in conductivity of 900% resulted in a maximum overall increase of heat flux of 395.39%.
5. Heat flux increased when specific heat increased. Overall, the heat flux increased 52% due to 275% increase in specific heat that it is important.
6. Latent heat of vaporization of liquid affects the vaporization process and heat transfer during spray cooling. Lower latent heat enhances the vaporization process and heat transfer. The heat flux increased approximately 21% due to decrease in latent heat around 83%.
7. The effect of thermal conductivity of liquid was most important for achieving high heat flux followed by specific heat and latent heat of vaporization.
8. The complex interaction of conduction of the heat from the heated surface into the liquid and convection of the liquid during sudden impact of a droplet or breaking of the vapor bubble and formation of the vapor bubble due to phase change were identified to be the major phenomena in spray cooling.
9. The importance of quick removal of the hot liquid from heated surface and moving the cooler liquid quickly to the heated dry surface which causes the high heat flux due to transient conduction was also recognized. This was illustrated with fluid flow visualization, temperature contour and heat flux (q) plots at different time instants. Understanding of this high heat transfer mechanism is very useful to design efficient thermal management system.

Sub-task 2.2: Experimental Results Using Spray Cooling

Survey of Multiple Nozzle Spray Systems

Previous research work on spray cooling techniques has used commercial nozzles [2.14][2.15]; unfortunately, these nozzles require more volume. Nozzles made in house were investigated by Lin et al. [2.4][2.16-2.18] to reduce the volume for removing heat from large areas. They developed a miniature nozzle array with 8 (2 x 4) nozzles for 2 cm^2 (1 x 2 cm^2) surface area and studied critical heat flux (CHF) for different nozzle pressure drops and different liquids. They found that spray cooling can reach CHF levels of 91.5 W/cm^2 with FC-87, 83.5 W/cm^2 with FC-72 and 490 W/cm^2 with methanol. Lin et al. [2.18] designed a miniature nozzle array with 48 (4 x 12) nozzles to cool a larger area (19.3 cm^2, i.e., 2.54 x 7.6 cm^2). They found that the CHF for this array is 34% lower than their previous study [2.4][2.16-2.17]. In this study they also investigated the effect of different nozzle pressure drops and found that the heat flux increases are small with increases in nozzle pressure drop at nozzle pressures of 1.72 bars.

Horacek et al. [2.19] studied time and spaced resolved heat transfer data on a nominally isothermal surface cooled by 2 spray nozzles. The distance between nozzle and heated surface is varied from 7 to 17 mm. They found a maximum heat flux of 66 W/cm^2 using FC-72 as cooling liquid. They concluded that the heat flux became more uniform across the heated surface as the spray distance was increased. From the design perspective, this implied that there is likely an optimum spray distance if one wishes to achieve uniform heat flux distribution. This may not be the same optimum distance if one wishes to

achieve the maximum heat removal rate from the heated surface. Pautsch et al. [2.20] designed the nozzle arrays ranging from 1 to 16 nozzles of swirl-chamber type pressure atomizers to cool an area of 49 cm^2. They tested ten different nozzle array designs.

Multiple Nozzle Spray Design at UA Using Innovative Fluid Removal Array

From the computational modeling research at the University of Arkansas (UA), transient conduction found to be the main mechanism for achieving high heat transfer. According to this mechanism, heat transfer can be improved if the bubble and stagnant hot liquid is removed quickly from heated surface and fresh cold liquid comes in contact with the hot surface. Using the knowledge gained through the UA modeling work, a novel fluid removal array was designed that can be an attractive solution for cooling of large areas. A detail of the fluid removal system is discussed in the following section.

Liquid Removal

A novel idea is introduced here to remove the liquid stagnating between the sprays as shown in Fig. 2.1 to Fig. 2.3. The removal points are set close to the heated wall to control the liquid film surface. The removed liquid from the surface is compactly transported via a pipe network between the nozzles and finally through a manifold on one side. The spray volume is also controlled by a spray cone region. This invention reduces the free space volume and hence the pumping system may be efficient. The advantage of this invention is that the cooling system is compact and efficient. The prototype device incorporates integral removal pathways and cone guides.

The stagnated liquid between the spray regions is removed with the removal points set close to the heated surface to control the thickness of the liquid film on the heated surface. The space outside the spray cone is eliminated by using the space for removing the liquid as well as reducing the free space volume. By reducing the free space the spray process is controlled much better. Once the liquid is removed they go through a network of pipe system between nozzles and are removed by a manifold on one of the sides.

Fig. 2.1 illustrates where the liquid enters the plenum of the spray chamber and enters into the nozzle; these are marked in green color. Then the liquid from the spray region on the hot plate is vertically removed as shown in red arrows at the bottom and then it gets collected via pipe network and then out of the box via an outlet. The heat source is at the bottom. Fig. 2.2 details the dimensions used in the spray system for spacing the spray nozzles (0.25 inches), clearance around the nozzle diameter (0.0938 inches), fluid removal pipe from the spray region (0.04 inches in diameter), spray region (0.3 inch diameter) and spray cone height (0.375 inches). The outlet pipe diameter is 0.25 inches. Fig. 2.3 illustrates more details of the liquid removal system.

The dimensions shown in the prototype is to illustrate the concept. The invention here is the concept of removing the stagnant fluid between the spray/jet region, the cone guides for the spray nozzle and the pipe network running between the nozzles to remove the effluent liquid. The liquid removal array can be used with and without the spray cone and spray nozzles.

Nozzle Array

In this regard, the spray nozzles developed by Lin and Ponnappan [2.4] from the US Air Force were successfully implemented in an area of 4 cm^2. When Lin et al. [2.18] extended their spray nozzle array from 2x4 to 4x12 they found that heat flux was reduced by 30% to 40%. This may be due to stagnation of the liquid in between the nozzles as a result of spray interaction. UA researchers are proposing utilization of a novel technique to remove the stagnating fluid efficiently as discussed earlier.

Volume

Most of the available spray systems are using commercial spray nozzles and they generally occupy large volumes. Only few used multiple nozzles. Under the UA invention, multiple nozzles are arranged in a compact form that requires less volume (2 in x 1.625 in x 0.375 in) as shown in Figs. 2.2 and 2.3. The existing technology in removing the sprayed liquid is to remove from the sides.

An invention was disclosed to the University officials for possible patenting.

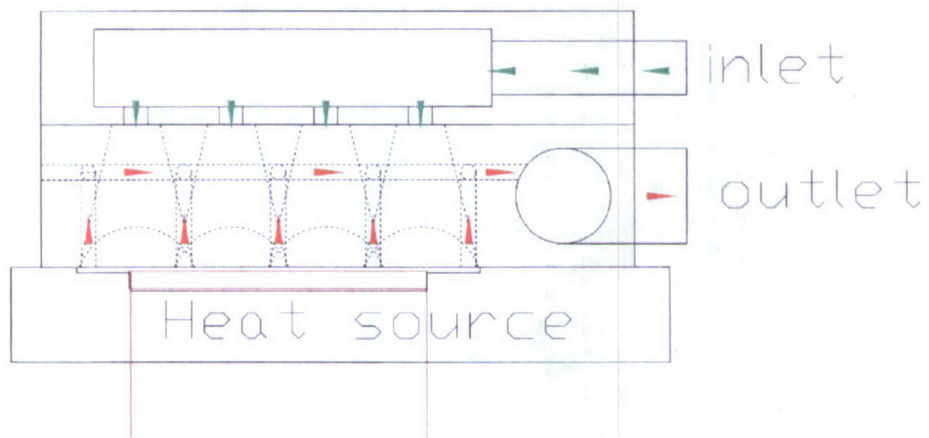

Fig. 2.1 Cross section of the spray cooling device.

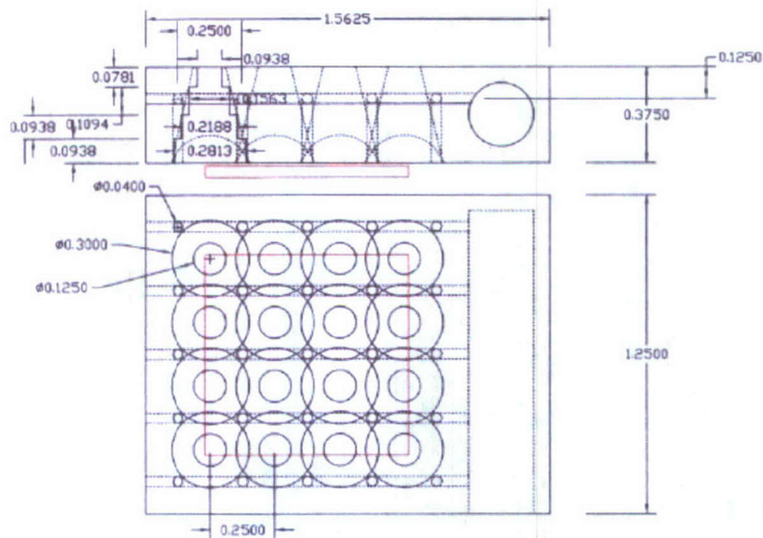

Fig 2.2 Plan and cross section of the spray cooling device detailing the fluid removal array.

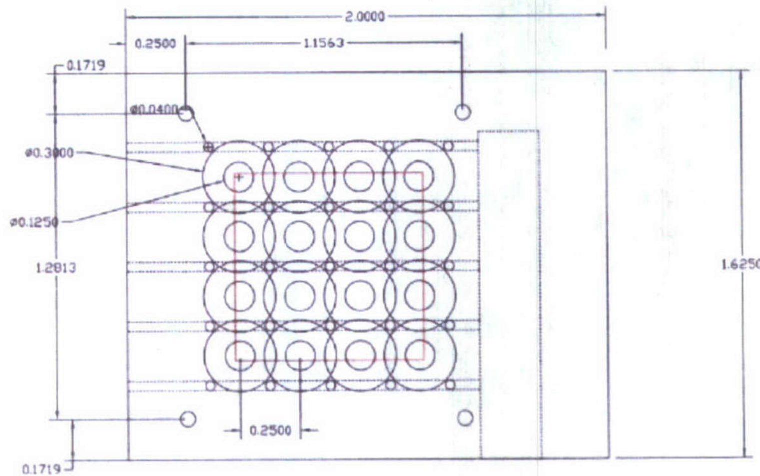

Fig 2.3 Plan view of the spray and liquid removal regions.

Spray-Cooling Experiments and Results

The experimental setup is designed to measure the heat flux and critical heat flux (CHF) for the multiple-nozzle system. The schematic representation of the test setup is shown in Fig. 2.4. The system consists of the multi nozzle plate, a spray box with effluent removal system, a heater assembly, a reservoir, a gear pump, a water chiller to control the liquid temperature and a filter. The jet impingement box is connected to the surface of the heater assembly. The distance between the nozzle orifice and the cooling surface is 8.8mm. The working fluid is FC-72. The pump is used to generate the pressure difference to maintain the circulation flow. The sub-cooled liquid droplets are impacting on the heated surface through the nozzle orifices and the spent liquid removal ports are sucking the liquid from heated surface uniformly. A part of the liquid forms a thin film over heated surface, a part of the liquid vaporizes and a continuous liquid flow occurs from the impacting region to the removal area and the removal ports. The vapor also flows along with the liquid out of the chamber through the spent liquid removal ports and pipe network which guides the two-phase flow to the water chiller where the liquid exchanges the heat. The liquid is finally coming back to the reservoir and again flows through the inlet pipe of the spray box. The flow rate is measured using a flow meter. The nozzle pressure drop (the pressure difference between the inlet pressure and spray/jet impingement chamber pressure) is controlled by the pump. The power input is proportional to the pressure difference between inlet and outlet. The inlet and outlet temperatures of the liquid are measured by T-type thermocouples (T3 and T4 in Fig. 2.4).

The experiments were performed for two different flow rates and liquid temperatures using FC-72 as the coolant. The results are presented in Figs. 2.5 and 2.6. The saturated temperature of the liquid is 53^0 C. Generally, the heat flux increases with superheat, $T_w - T_{sat}$. For a given superheat, heat flux increases with volumetric flow rate and lower liquid temperatures. As seen from the figures, the slope of the heat flux curve varies with superheat. In the lower superheat region, the slope is relatively small and does not change much. In this case, the heat transport is mainly due to convection and conduction. As superheat exceeds a point, around 17^0C, the slope of the heat flux curves increases and then starts to decrease. This trend indicates that two phase is becoming a major part of the heat transfer mechanism. Heat transport in this region involves more convection, evaporation of the liquid and transient conduction. It is further observed that the two-phase heat transfer starts at lower superheat and critical heat flux is reached at lower superheat for lower flow rates than higher flow rates. Maximum heat flux is found to be 72 W/cm^2 for a flow rate 0.8 L/min and liquid temperature of 30^0C. This heat flux is higher than the heat flux obtained for the large-area spray cooling array of Lin et al. [2.18].

Fig. 2.4 Schematic view of the experimental setup.

Fig. 2.5 Heat flux curve for different flow rates.

Fig. 2.6 Heat flux curve for different liquid temperatures.

Sub-task 2.3: Experimental Results Using Liquid Jet/without Spray Nozzle System

General Description

The same effluent fluid removal array is used to study the heat transfer phenomena for a cooling system using an array of liquid jets replacing the nozzles in above discussed system. In this case, everything was same as the spray cooling experiments of the previous sub-task except the spray nozzles that were removed. The spray nozzle array was replaced by an array of liquid jet orifices. This system looks like Fig. 2.7, two different hole sizes are placed in the jet orifice plate. The liquid volume coming from the orifices is not controlled by any cone region here. In this case, one set of holes with the same size (diameter 0.063 inches) acts as jet orifice and another set of holes with the same size (0.052 inches) acts as suction holes or removal ports (Figs. 2.8 and 2.9). The removal ports are placed between jet orifices. The removed liquid from the heated surface is compactly transported via pipe network between jet orifices and finally through the manifold on one side as done in the previous sub-task. The jet orifices and suction holes are placed at same distance from the heated surface (upper right side of Fig. 2.7). The spacing of jet orifices is the same as in the spray nozzle system (i.e., same as nozzle orifice spacing of 0.25 inches). The jet orifices are designed as a 4x4 array with a diameter of 0.063 inches. The fluid removal (suction) orifices are also spaced as in the spray system (0.25 inches). In Fig. 2.7, Flow 2 represents reverse flow of Flow 1. Using the same jet plate, two different flows are created. For Flow 1, the coolant flows through 16 jet orifices (0.063 inches diameter) to the heated surface and the effluent liquid is sucked by 25 holes with diameter of 0.052 inches; whereas for Flow 2, the coolant flows through 25 orifices with diameter of 0.052 inches and effluent is sucked by 16 holes with diameter of 0.063 inches.

An invention was disclosed to the University officials for possible patenting.

Fig. 2.7 Schematic of jet plate and effluent removal system.

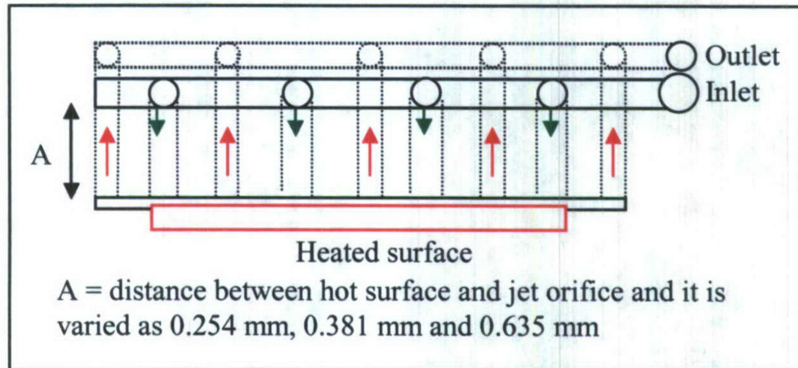

Fig. 2.8 Cross sectional view of the jet impingement device.

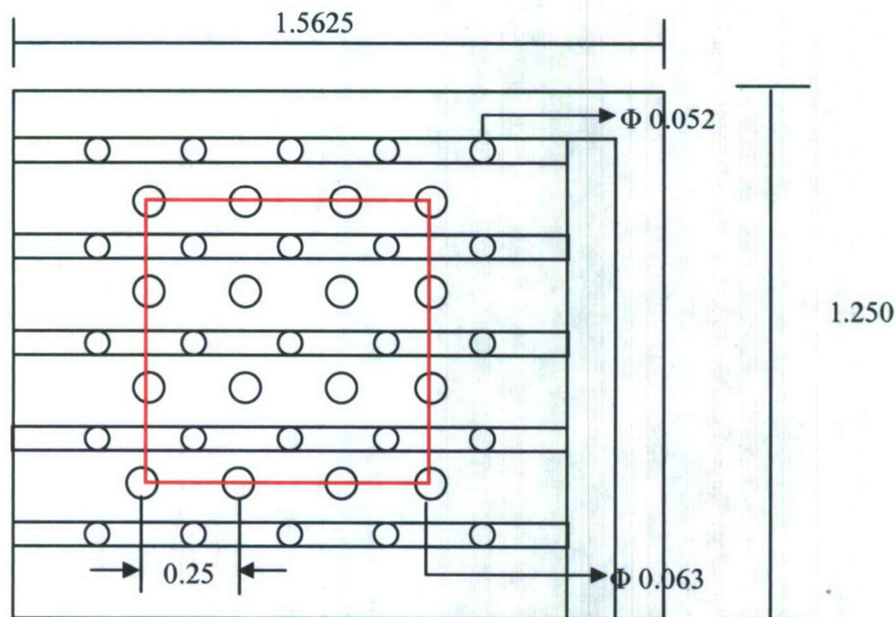

Fig. 2.9 Plan view of the jet impingement and fluid removal region.

Results and Discussions

The same experimental set up discussed in the above sub-task is used for these experiments; only the spray box is replaced by the jet impingement box. Three different values (i.e., 0.01 inches (0.251 mm), 0.015 inches (0.381 mm) and 0.25 inches (0.635 mm)) of the distance between the jet orifice and the hot surface A (shown on the right side of Fig. 2.8) were considered to investigate the distance effect on heat transfer. Furthermore, the experiments were performed for coolant flow rates of 1.25, 1.5 and 2.0 L/min and different liquid temperatures. The results are presented in Fig. 2.10 to Fig. 2.13.

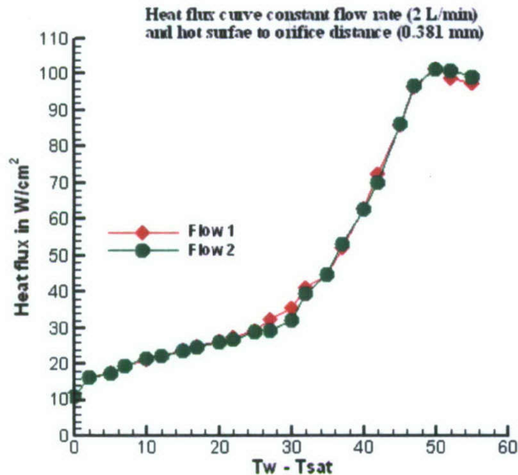

Fig. 2.10 Heat flux curve for two different flows at 2 L/min flow rate and hot surface to nozzle orifice distance of 0.381 mm.

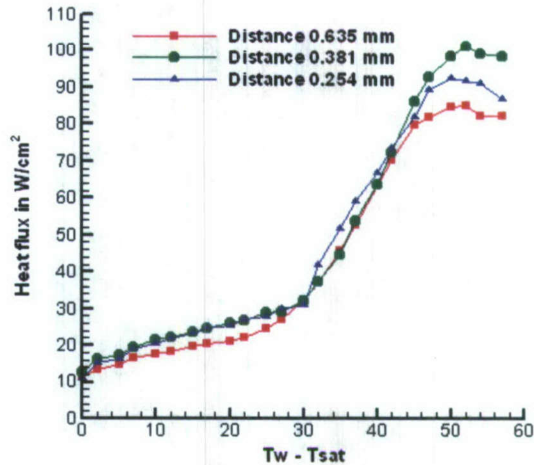

Fig. 2.11 Heat flux curve for different distances between jet orifice and hot surface at 2 L/min flow rate and liquid temperature of 23^{0}C.

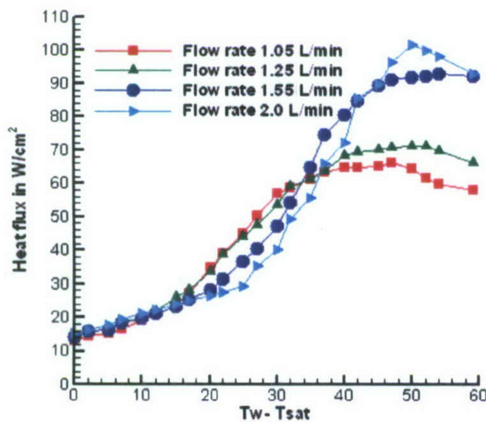

Fig. 2.12 Heat flux curve for different coolant flow rates at 23^{0}C liquid temperature and jet orifice to hot surface distance of 0.381 mm.

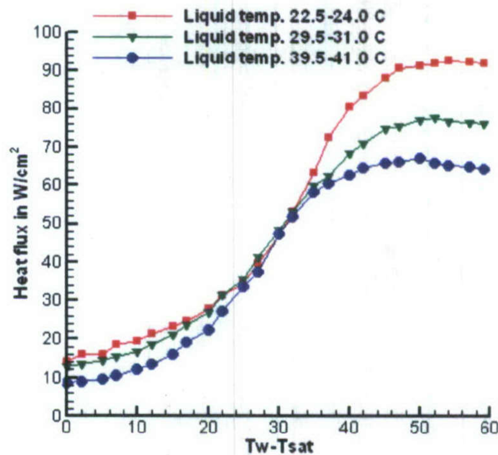

Fig. 2.13 Heat flux curve for different coolant liquid temperatures at constant flow rate 1.55 L/min and jet orifice to hot surface distance of 0.381 mm.

Fig. 2.10 indicates that the heat flux curve is the same for Flow 1 and Flow 2. Though the heat flux curve is same for Flow 1 and Flow 2 for same flow rate, the effective flow rate used to cool the heated surface is lower for Flow 2. Among 25 orifices, liquid flow coming from 9 orifices is used to cool the hot surface (Fig. 2.9). Other 16 orifices are flowing out of the heated surface area. Hence, less than 50% flow rate is used to cool the heated surface. From this study it is concluded that the distance between jet impacting locations to suction port locations is very important. As this distance is the same for both flows, the heat flux is the same for Flow 1 and Flow 2 though the effective flow rate is lower for Flow 2. It is believed that if this distance is shorter, the effluent liquid can be removed more quickly and higher heat fluxes can be achieved with a lower flow rate. In the future, a new jet plate will be designed with

shorter distance between jet impacting locations to suction port locations and heat transfer studies will be performed.

The results presented here are only for Flow 1 (Fig. 2.11 to Fig. 2.13). The general heat flux curve trend is similar to the heat flux curve discussed in the spray cooling results section. For a given superheat, heat flux increases when orifice to heated surface distance decreases from 0.025 inches to 0.015 inches (Fig. 2.11). When this distance decreases, the fresh coolant liquid can come in contact of the heated surface quickly resulting in higher heat fluxes. However, when the distance further decreases from 0.015 inches to 0.01 inches, the fresh liquid reach to heated surface more quickly but effluent fluid removal system becomes the limiting factor. Therefore, heat flux does not increase further. Hence, the optimum distance for this system is found to be around 0.015 inches. Fig. 2.12 shows that the critical heat flux increases with liquid flow rates. At lower superheat (until 10^0C), heat flux is similar for every flow rate. Two-phase heat transfer starts at lower superheat and critical heat flux is also reached at lower super heat for lower flow rates than higher flow rates. For a given superheat, heat flux increases when liquid temperature decreases (Fig. 2.13). When the liquid temperature is low, the temperature difference between the hot surface and the liquid is larger. This larger temperature difference results in high heat flux due to higher conduction and convection. For a particular superheat range, around 30^0C to 37^0C, the heat flux is the same for every liquid temperature. The heat flux in this region may be mainly ruled by nucleate boiling and resulting transient conduction. As the nucleation sites are constant for a particular surface, the heat flux is the same. The critical heat flux is higher for lower coolant temperature because of larger temperature difference between coolant and hot surface. Maximum heat flux is found to be 101 W/cm^2 for a flow rate 2.0 L/min and liquid temperature of 23^0C when the hot surface to jet orifice distance is 0.015 (0.381 mm) inches. This heat flux is higher than the heat flux found for spray cooling as discussed in previous sub-task. Some important parameters for cooling systems are tabulated in Table 2.1.

Table 2.1 Important parameters for multiple spray/jet cooling.

Researchers	**Year**	**Cooling system**	**No. of Nozzles/-jets**	**Nozzle Pressure Drop in bars**	**Area Used in cm^2**	**Achieved q in W/cm^2**	**Distance Between hot plate and nozzle/jet in mm**
Lin et al.	2002	Spray	8	1.03-2.41	2	83.5	8.8
Lin et al.	2004	Spray	8	0.69-3.10	2	83.5	8.8
Lin et al.	2004	Spray	48	0.69-3.10	19.3	60	10
Horacek et al.	2004	Spray	2	Not found	0.49	66	7-17
Pautsch et al.	2005	Spray	1-16	1.03-3.10	49	77.8	6.8
Selvam et al.	2008	Spray	16	N/A	4	72	8.8
Selvam et al.	2008	Jet	16	0. 4-0.7	4	101	0.381

Comparison of Cooling Systems between Spray and Jet/Without Spray Nozzles

The same fluid removal system is used for spray cooling and jet/without nozzle system with the critical heat flux found to be higher for jet system. Maximum obtained heat flux for jet/without nozzle system is 101 W/cm^2 whereas for spray/with nozzle system is 72 W/cm^2. The total cost to make the spray box is approximately $2500 that is much higher than the cost for the jet box (approximately $800). The volume of the spray box and jet box are the same. Overall, the jet/without nozzle system is very efficient and useful for large area cooling.

Summary and Conclusions

A novel effluent fluid removal array was designed using knowledge gained through computational modeling work. The new fluid removal array was implemented for closed-loop test of spray and jet impingement cooling. FC-72 was used as working liquid. For the jet impingement system, the jet orifices were placed very close to the hot surface (i.e., 0.254 mm – 0.635 mm). This small distance helps the fresh liquid to reach the hot surface quickly resulting in higher heat fluxes. In this system, the liquid film thickness can also be controlled.

The experiments were performed for different liquid temperatures and liquid flow rates. The effect of distance between the jet orifices and the hot surface on heat transfer was also investigated. The optimum distance was found to be around 0.025 (0.381 mm) inches. For a given super heat, heat flux increases with decrease in liquid temperature. The critical heat flux increases with liquid flow rate. Highest heat flux was observed as 101 W/cm^2 for a liquid flow rate of 2 L/min and a liquid temperature around 23^0C for a hot surface to orifice distance of 0.381 mm. Advantages of this system are that the energy consumption to maintain the pressure difference between inlet and outlet for a given liquid flow is smaller than the energy required by other approaches, the system volume is also smaller, and the maximum heat flux is as high as 101 W/cm^2 using FC-72 as coolant. Overall, the system is very cost effective and useful for large area cooling.

Further studies can be conducted for further lower liquid temperatures and higher flow rates. As the fluid removal ports are placed uniformly over the area, it will remove similar heat fluxes from even larger areas. However, the cooling system should be tested for very large areas. The effect of distance between jet orifices to suction ports can be investigated. Another pump can be used at the outlet side of the jet impingement box to suck the effluent fluid more quickly. Quick removal of the effluent fluid can result in higher heat fluxes. The fluid removal ports and jet orifices can be placed in different horizontal planes and the optimum distances of suction ports to hot surface, and of jet orifices to hot surface can be separately obtained.

References

[2.1] J. Yang, L.C Chow, and M.R. Paris, "Nucleate Boiling Heat Transfer in Spray Cooling", *Journal of Heat Transfer*, 1996, vol. 118, pp. 668-671.

[2.2] L.C. Chow, M.S. Sehembey and M.R. Paris, "High Heat Flux Spray Cooling", *Ann. Rev. Heat Transfer*, 1997, vol. 8, pp. 291-318.

[2.3] I. Mudawar, "Assessment of High Heat-Flux Thermal Management Schemes", *IEEE Transactions on Components and Packaging Technologies*, 2001, vol. 24, pp. 122-141.

[2.4] L. Lin, and R. Ponnappan, "Heat Transfer Characteristics of Spray Cooling in a Close Loop", *Int. J. Heat Mass Transfer*, 2003, vol. 46, pp. 3737-3746.

[2.5] S. Jiang, and V.K. Dhir, "Spray Cooling in a Closed System with Different Fractions of Non-Condensable in the Environment", *Int. J. of Heat and Mass Transfer,* 2004, vol. 47, pp. 5391-5406.

[2.6] R.P. Selvam, "Numerical Modeling of Spray Cooling Phenomena for Thermal Management of High Power Systems", *Report to Universal Technology Corporation*, Dayton (OH), August 2004.

[2.7] R.P. Selvam, L. Lin, and R. Ponnappan, "Computational Modeling of spray Cooling: Current Status and Future Challenges", *Proceedings of the Space Technology and Applications International Forum (STAIF)*, Conference on Thermophysics in Microgravity, Albuquerque (NM), Feb. 13-17, 2005.

[2.8] R.P. Selvam, S. Bhaskara, J.C. Balda, F. Barlow and A.Elshabini, "Computer Modeling of Liquid Droplet Impact on Heat Transfer During Spray Cooling", *ASME Summer Heat Transfer Conference*, San Francisco (CA), July 17-22, 2005, paper no: HT2005-72569.

[2.9] R.P. Selvam, M. Sarkar and R. Ponnappan, "Modeling of Spray Cooling: Effect of Droplet Velocity and Liquid to Vapor Density Ratio on Heat Transfer", *16th Annual Thermal & Fluids Analysis Workshop*, Orlando (FL), Aug. 8-12, 2005.

[2.10] R.P. Selvam, M. Sarkar, S. Sarkar and R. Ponnappan, "Effect of Vapor Bubble Size on Heat Transfer in Spray Cooling", *Space Technology and Applications International Forum (STAIF)*, Conference on Thermophysics in Microgravity, AIP Conference Proceedings, Albuquerque, NM, Feb. 12-16, 2006, vol.: 813, pp 145-152,

[2.11] R.P. Selvam, L. Lin, and R. Ponnappan, "Direct Simulation of Spray Cooling: Effect of Vapor Bubble Growth and Liquid Droplet Impact on Heat Transfer", *Int. J. of Heat and Mass Transfer*, 2006, vol. 49, pp. 4265-4278.

[2.12] R.P. Selvam, M. Sarkar, and R. Ponnappan, "Effect of Thermal Conductivity and Latent Heat of Vaporization of Liquid on Heat Transfer in Spray Cooling", *Proceedings of SAE Power system conference*, New Orleans, LA, November 7-9, 2006.

[2.13] M. Sarkar, "Multiphase Flow Modeling of Spray Cooling to Improve Heat Transfer", *PhD Dissertation*, University of Arkansas, 2008.

[2.14] K. Vanam, J. Junghans, F. Barlow, R. P. Selvam, J. C. Balda and A. Elshabini "A Novel Packaging Methodology for Spray Cooling for Power Semiconductor Devices Using Dielectric Liquids", *IEEE 2005 Applied Power Electronics Conference (APEC'05),* Austin (TX), March 6-10, 2005, Vol. 3, pp. 2014-2018

[2.15] B.L. Rowden, R.P. Selvam and E. A. Silk (2006), Spray Cooling Development Effort for Microgravity Environments", *Proceedings: Space Technology and Applications International Forum (STAIF)*, Conference on Thermophysics in Microgravity, *AIP Conference Proceedings*, Albuquerque, NM, Feb. 12-16, 2006, Vol.: 813, pp 134-144,.

[2.16] L. Lin and R. Ponnappan, "Critical Heat Flux of Multi-Nozzle Spray Cooling in a Closed Loop", 37th Intersociety Energy Conversion Engineering Conference, Washington D.C., July 29-31, 2002.

[2.17] L. Lin and R. Ponnappan, "Critical Heat Flux of Multi-Nozzle Spray Cooling", *Journal of Heat Transfer*, 2004, vol. 126, pp. 482-485.

[2.18] L. Lin, R. Ponnappan, K. Yerkes and B. Hager, "Large Area Spray Cooling, paper: AIAA 2004-1340, 42nd AIAA Aerospace Sciences Meeting & Exhibit, Reno, Nevada, Jan. 5-8, 2004.

[2.19] Horacek, B., Kim, J. and Kiger, K.T., "Spray Cooling Using Multiple Nozzles: Visualization and Wall Heat Transfer Measurements", *IEEE Transactions on Device and Materials Reliability*, 2004, vol.4, pp. 614-622.

[2.20] A.G. Pautsch, and T.A. Shedd, "Spray Impingement Cooling with Single and Multiple Nozzle Arrays. Part I: Heat Transfer Data Using FC-72", *International Journal of Heat and Mass Transfer*, 2005, vol. 48, pp. 3167-3175.

Task 3: Development of Spray Cooled Power Modules

The technical leader of this task was Dr. Fred Barlow until moving to the University of Idaho in July 2006. Afterwards, Mr. Brian Rowden assumed the leadership of the remaining activities with support from Dr. Juan Carlos Balda.

The activities performed under this task could be divided into three sub-tasks; namely

- Sub-task 3.1: Packaging of SiC Diodes
- Sub-task 3.2: Investigation of High-Temperature Die Attach Materials
- Sub-task 3.3: Spray-Cooled Power Conversion Modules

Sub-task 3.1: Packaging of SiC Diodes

This sub-task was led by Dr. Fred Barlow who supervised the packaging of silicon carbide (SiC) 75-A diodes by his doctoral student Kiran Vanam. These bare dies were obtained through a contract with the DoE Oak Ridge National Laboratory.

Introduction
Recent demand for SiC electronics, operating at high temperatures (above 200ºC), has significantly increased at various sectors (e.g., automotive, energy, military, aerospace, radar and communication). The limitations of the silicon-based device technology for high-temperature applications has propelled the demand for alternative materials such as diamond, silicon carbide (SiC), gallium nitride and aluminum nitride – wide band gap materials. The exceptional material properties of these materials such as resistance to radiation, chemical inertness, high breakdown electric field, high thermal conductivity etc have made them viable options for harsh operating environments [3.1]. Out of the mentioned wide band gap materials, SiC processing technology is the most advanced and therefore it stands a better chance for meeting the current high-temperature requirements [3.2][3.3]. SiC is attractive as it has higher thermal conductivity than silicon and aids in the thermal management problem if the rest of the package thermal resistance is minimal. Thus, the benefits offered by SiC device technology can only be reaped by concurrent developments in the area of packaging. Lack of reliable packaging methodologies for high temperature regime (200ºC) hinders the commercial acceptability of high temperature electronics [3.4] [3.5]. Thus advancements in packaging area are quite essential for meeting the demands of various sectors in the industry and military. At present, only SiC Schottky diodes and JFETs are commercially available. Other power devices are in their developmental stage with Cree Inc (Raleigh, NC) promising to make SiC MOSFETs commercially available in early 2009. Finally, device manufacturing costs for SiC are more than Si but these should decrease as the manufacturing technology for the wideband gap devices matures; in particular, if there are more vendors of SiC substrates, the component representing a significant part of the device cost.

In this work a flip chip variation of a power package that can be spray cooled using water is proposed. The viability of the proposed package was first implemented on a Si-based 16A, 600V diode because of its availability in large numbers in bare die form. The material selection and the packaging technology were vital for the high temperature and high voltage operation of the package. After successful implementation, this packaging concept was applied to a SiC-based 75A, 1200V diode from Cree.

Proposed Packaging Concept for Spray Cooling with Water

A flip-chip power package is shown in Fig. 3.1 consisting of a DBC hat that forms the top side anode connection of the diode, and DBC substrate forms the bottom side cathode connection. The Kovar legs complete the connectivity between the hat and the DBC substrate. A temperature hierarchy in solder selection is a key in realizing the package. Medium temperature (<300°C) 95/5 PbSn (lead-tin) solder balls form the top side anode connection and 2 mil thick Indium alloy 209 preform (65Sn 25Ag 10Sb) was utilized for bottom side device and base plate attachment. Alloy 209 has a melting point of 233°C and once it melts forms an alloy with the base metal on to which it reflows and subsequent reflow will be around 265°C. Another alloy that is suitable for base plate attachment was Indium alloy 121 (96.5Sn 3.5Ag), which has a reflow temperature of 221°C. Alloy 121 is a very good stress absorber and can be used with pure copper base plate as opposed to expensive AlSiC or CuMo base plates. It also has very good thermal conductivity, high fatigue and creep resistance, as well as high tensile strength.

For the proposed package, the major thermal conduction path is via the device, DBC substrate and Cu base plate. When using water, the spray should be directed onto the base plate over the areas where the device is located via nozzle(s) mounted to a nozzle manifold. A slight over spray might be necessary due to the thermal spreading in DBC and Cu Base plate. The manifold is bolted to the base plate of the module and is sealed with an O-ring arrangement. The proposed concept is illustrated in Fig. 3.2.

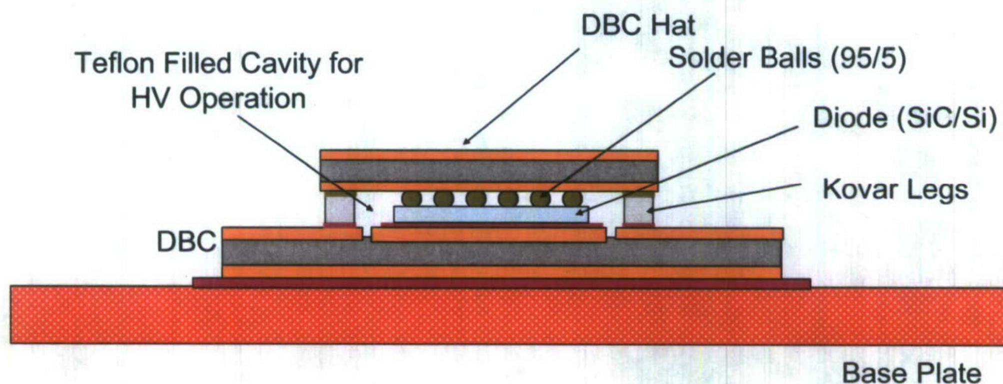

Fig. 3.1 Proposed flip chip variation of the power package compatible with spray cooling using water.

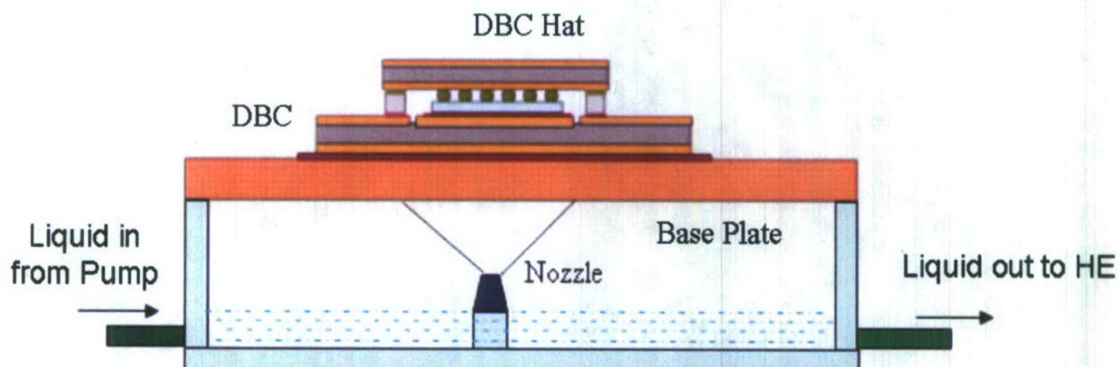

Fig. 3.2 Schematic of spray cooled flip chip power package.

Processing of the Si Based Flip Chip Power Package (Single Diode Package)

The feasibility of the packaging methodology was first implemented using a Si-based 16A, 600V diode from International Rectifier. The diode was intended to be packaged by using conventional wire bonding technology. Therefore, the top metallization (anode) was 99% Al 1% Si and the bottom metallization was Cr-Ni-Ag that can be soldered to a substrate using conventional solders, refer to Fig. 3.3. Since the flip-chip operation requires solderable metallization on both sides of the device, the top metallization was electroless nickel (EN) plated. The EN plating involves a zincating step which removes the native oxide present on Al and coats base metal with a thin layer of zinc. Later when the zincated diode is immersed in the EN plating solution, the zinc is etched away and around 4 µm of Ni is plated on to Al. The thickness of Ni layer depends on the time that the device is left in the bath and deposition rate was approximately 0.5 µm/min. Around 5 µm of benzo-cyclo-butane (BCB), which acts as a solder mask on the die was deposited and patterned to yield 9 mil openings with a center to center pitch of 16 mils. In order to form the top side connections, first medium-temperature solder balls (95/5 PbSn) were reflowed on the diode as shown in Fig 3.4. DBC substrate, DBC hat with solder mask matching the die, power terminals and Kovar legs were machined and processed before assembling the complete package. First the diode with the solder balls was flipped on to the DBC hat and reflowed along with the Kovar legs. Later this assembly was attached to the DBC substrate using 65Sn 25Ag 10 preform. The completed assembly is shown in Fig. 3.5. The completed package successfully passed the electrical test which proved the packaging methodology. Careful selection of the materials with matched CTEs and dimensions were critical for the success of the package.

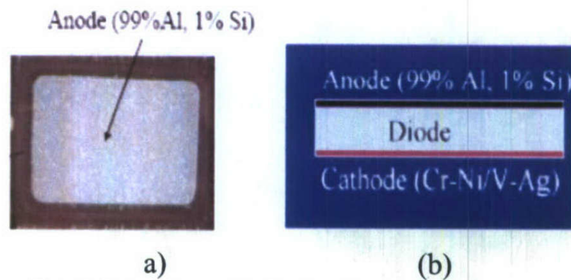

a) (b)

Fig.3.3 (a) Bare Si diode, (b) Sectional view.

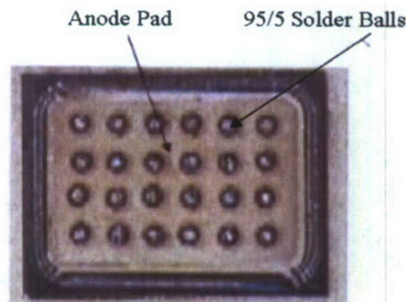

Fig. 3.4 Solder balls reflowed on the diode.

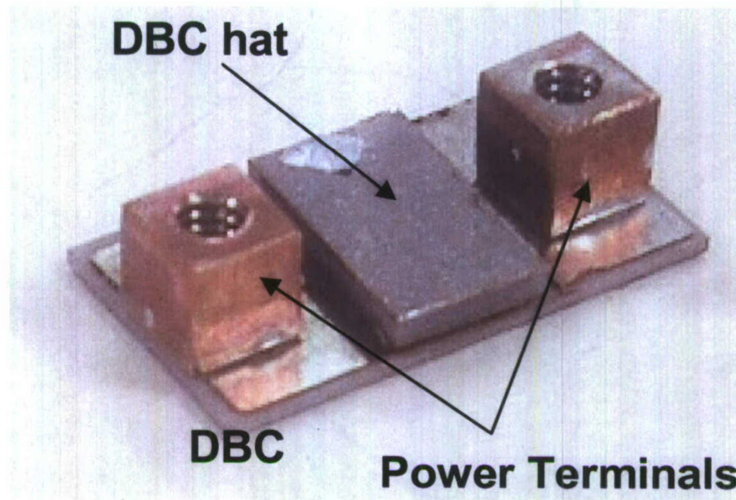

Fig. 3.5 A Si diode packaged using the proposed packaging technique.

(a)

(b)

Fig. 3.6 (a) Zincated SiC diode, (b) EN plated SiC diode.

Processing of the SiC Based Flip Chip Power Package (Single Diode Package)

Researchers with DoE Oak Ridge National Laboratory contracted with Dr. Fred Barlow the packaging of a single SiC-based 75A, 1200V bare die diode using the packaging concept presented in the previous section. This SiC diode was manufactured by Cree Inc (Raleigh, NC).

The devices had Al on the top side (anode) and Ni on the bottom side (Cathode) requiring additional processing. The top side was EN plated as described earlier. The zincated and EN plated diode is shown in Fig. 3.6. The next step was to deposit solder mask using BCB and the problem of handling individual bare diodes was resolved using a thermal release tape during depositing and patterning BCB. Fig. 3.7 shows the SiC diode with 95/5 PbSn reflowed solder balls. There were more than 100 solder balls to handle the ampere rating of the device. The rest of assembly parts are shown in Fig. 3.8.

The solder balls were attached to the DBC hat by again reflowing the solder balls and Kovar legs using 2 mil 95/5 preform. The DBC hat along with the SiC diode was attached to a DBC substrate using indium alloy 209. The Cu base plate (125 mils thick) was also reflowed during this time. The completed package, shown in the Fig. 3.9, is similar to the Si-based package but smaller.

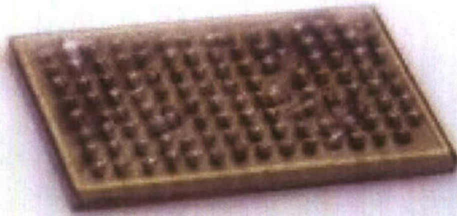

Fig. 3.7 SiC diode with medium temperature solder balls.

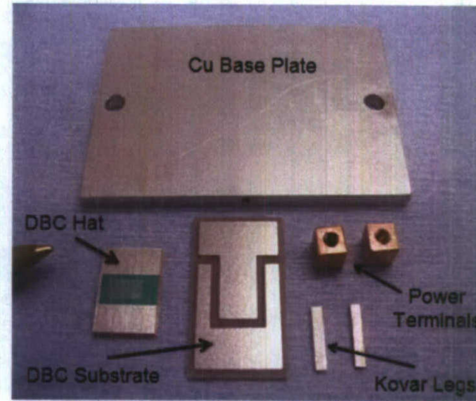

Fig. 3.8 The parts of the assembly.

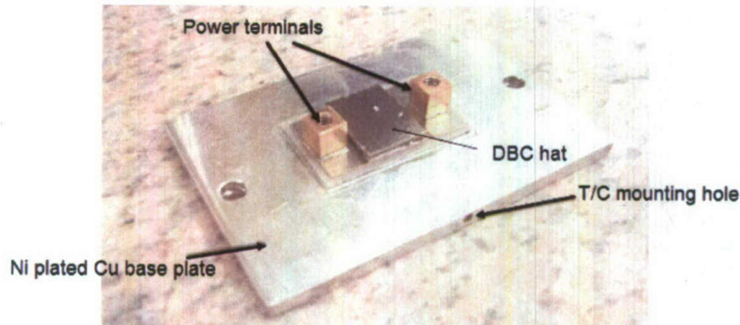

Fig. 3.9 Completed SiC flip-chip package.

The proposed package is capable of handling temperatures around 200°C and high voltage operation is possible by filling the gap between the top DBC hat and the substrate with Teflon. The package was tested using a cold plate to confirm the feasibility of the package for handling the high current. The base plate of the SiC package was bolted to the heat sink and thermal grease was used to fill the gap between the base plate and cold plate. The test setup and the diode I-V curves are shown in Fig. 3.10.

Conclusions

The work reported in this sub-task has demonstrated the successes of the packaging methodology and associated selection of materials. The flip chip package represents the potential to further increase the packaging density for SiC devices as well as reducing parasitic effects related to long wire bonds and large traces needed to route the power through the module. This approach could also be expanded to dual sided cooling either active or passive in addition to advances in interconnect technology beyond solder balls. Currently, manufacturers of SiC devices are specifying current densities of 100 A/cm^2 when the devices are capable of 200 A/cm^2 or even higher because of device voltage drop considerations, but also package thermal resistance as it relates to maximum junction temperatures. There is a need to remove higher heat fluxes as the device current and package power density is increased. The proposed flip-chip packaging methodology, though more complex than using traditional wire bonding, combined with spray cooling could provide a thermal management solution enabling to increase the current density of SiC devices to 200 A/cm^2 or even higher as well as improved package performance with reduced parasitic effects and increased power density.

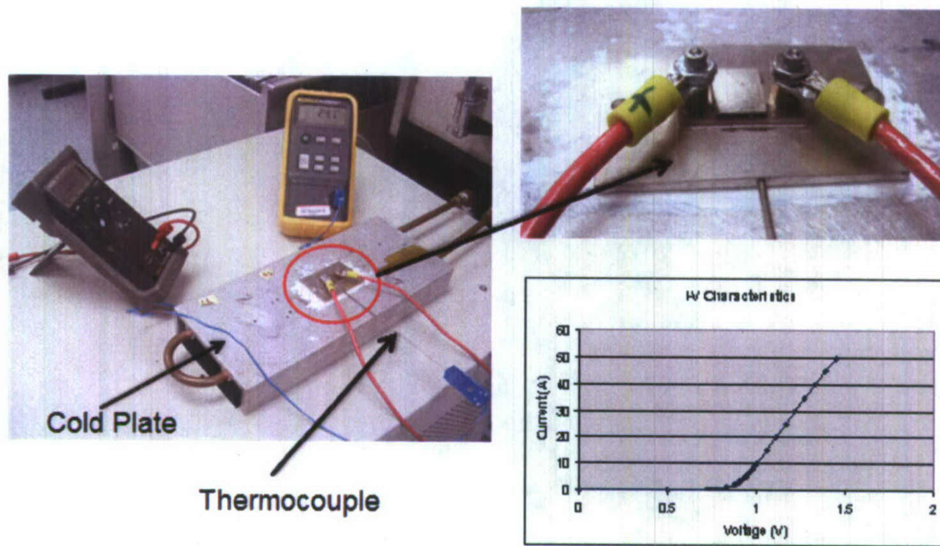

Fig. 3.10 Test setup and I-V characteristics of the SiC diode.

Sub-task 3.2: Investigation of High-Temperature Die Attach Materials

This work was performed by Mr. Brian Rowden and supervised by Dr. Barlow.

Introduction

The motivation for this research was a result of current silicon carbide (SiC) device development, and the subsequent need for suitable packaging alternatives. The primary interest for this sub-task was in *high temperature applications* defined as operating temperatures at or above 300°C. In particular, the focus was in relation to die attach materials while realizing that needs for suitable lead frame, lid seal, or second level assembly alternatives also exist.

With current silicon technology, standard operating temperatures reside below 150°C resulting in the use of attachment methods with lower melting points than those required for SiC technology. Materials are employed in the case of silicon during packaging processes to create a temperature hierarchy bearing in mind the 150°C operating upper limit. Thus, high-temperature materials are currently available that can withstand the 300°C threshold though some are only capable for short time intervals. Therefore, the primary properties necessary for successful die attach are discussed first in this report including the common impact of the attachment materials. Then, materials are broken into families to discuss common chemistry, bonding mechanisms, and properties. Lastly, a more detailed evaluation of possible materials and approaches are addressed in detail.

Material Property Compatibility

As mentioned above, the analysis is focused on high temperature die attach materials concerning a SiC device attached to a ceramic substrate. To maintain the integrity of the bond, the properties of the die attach material need to be compatible with both the die and substrate. This section briefly outlines some general properties of substrate materials as they relate to critical processing properties. A primary advantage for the use of SiC devices is their capability of operating up to the 600°C range. This exploitation of SiC properties could also be extrapolated to the die attach methodology. Increasing the temperature above 300°C requires the *use of controlled atmosphere* in order to eliminate oxidation of the metallization on the substrate, die, and die attach material. This has not been the case with some of the

lower temperature alternatives (used for silicon technology) where the additional cost of a highly controlled environment have eliminated some viable and potentially better solutions.

The substrates discussed in this section focus on ceramic materials, including alumina, aluminum nitride, and glass ceramic, for potential applications up to 850°C. The typical physical properties for these materials including SiC are shown in Table 3.1 [3.6].

Table 3.1 Bulk material properties.

Bulk Material Properties	Density	Thermal Expansion	Thermal Conductivity	Flexural Strength	Young's Modulus	Dielectric Constant
	g/cc	ppm/°C	W/m-K	MPa	GPa	1 MHz
Silicon Carbide (SiC)	3.20	4.50	490	552-862	414-445	
Alumina 99.5% (Al2O3)	3.90	7.40	35	552	372	9.9
Alumina 96% (Al2O3)	3.75	7.50	26	400	303	9.5
Aluminum Nitride (AlN)	3.25	4.40	50-170	235-370	260-350	
Silicon Nitride (SiN)	3.18	3.25	7-30	450-800	310-330	8.8
Glass Ceramics	2.5 - 3.0	3.0 - 7.0	1-5	140		4 - 9
Mullite	2.82	3.70	4	186	50-220	5.4

With this wide temperature window (greater than 300°C), one of the most important properties for die attach material is thermal expansion. Ideally, the materials selected would be matched closely to eliminate inducing thermal stresses, or the more fragile die material would be placed in compression after attachment. For the ceramic substrates selected, the values for the thermal expansions are reasonably close, with *most die attach materials having a higher and often non-linear thermal expansion* than any of the materials listed in Table 3.1. An inherent issue with ceramic materials is the mechanical modulus and strength due to the brittle nature of the crystal structure. This is especially important for SiC devices as the bulk modulus and strength values are comparatively higher than the potential substrate materials. Some die attach materials also have a considerably high modulus that will need to be considered when selecting a substrate material. For high temperature and high power applications, thermal conductivity is also a primary concern. Silicon carbide possesses a high bulk thermal conductivity that allows for heat transfer rapidly from the die. For the most part, this heat will need to travel through the die attach material and the substrate to some sort of heat sink; therefore, serious consideration should be devoted to choosing the appropriate substrate and die attach materials and thicknesses to balance thermal and mechanical properties. Though not discussed in this report, the dielectric constant and voltage breakdown will also play key roles in the selection of a material especially in relation to high frequency and high power.

Material Descriptions

The term *die attach material*s is utilized in this report due to the variety of materials that can be employed in this process. The one common thread among all of these materials as they relate to this report will be electrical conductivity necessary to provide either signal or ground connection depending on the device. The need for electrical conductivity of the die attach material results in the need for a

direct metallic bond as in a solder or braze or a metallic filler incorporated into a base product as is the case with epoxies and filled glasses. In order to adequately discuss the merits of these different materials, each material system along with key characteristics and properties will first be defined. This will be followed by several in depth discussions of specific materials from each group suitable for the high-temperature focus of this activity.

One of the most common die attachment methods involves the use of direct bonding commonly referred to as soldering or brazing. The primary distinction between soldering and brazing is the processing temperature. Both processes use a filler metal or alloy that forms intermetallics with the adjacent metal systems. It is understood that the substrate materials must be able to sufficiently handle the temperature required for melting the filler metals. In each case, fluxes may be used to assist in surface cleaning and wetting. The breakpoint for the liquidus temperature is 450°C, above which it is a braze and below which it is a solder [3.7]. The following paragraphs will be evaluating solder, brazing, filled-glass and polymer materials.

Solder Materials

These find applications in all areas of electronics from automotive to aerospace to toaster ovens. Solder reflow temperatures can range from 10°C to the defined value of 450°C. The most typical alloys used for electronics are tin lead alloys or an equivalent replacement for environmental reasons. Solder compositions are designated as hard (AuSn) and soft (PbSn) solders based on their modulus and tensile strength. The temperature capabilities of a solder composition are limited by the constituent components of the alloy or pure metal as the case may be. In the case of lead tin, the melting points of the pure metals are 327°C and 232° for lead and tin, respectively. The most common compositions are the eutectic composition at 183°C relating to 63/37 SnPb and a higher temperature alloy around 310°C relating to 95/5 PbSn. For the purpose of packaging SiC devices, the lead tin system *does not* provide adequate temperature resistance for 300°C and above temperatures. The three main high temperature solders are gold tin, gold germanium, and gold silicon. All of these systems represent hard solders and are eutectic based. These materials will be analyzed in the next sub-section.

Brazing Materials

These are used in a variety of applications ranging from aerospace jet turbine engines to high temperature co-fired ceramic packages (HTCC) with brazing temperatures up to 1800°C. The most typical brazes for the electronics industry are silver based in order to reduce the overall processing temperature. In HTCC applications, brazes are used to apply leads and seal rings prior to die attachment. The used standard material is a silver copper eutectic or trade name Cusil® [3.8] comprised of 72% Ag and 28% copper and having a liquidus temperature of 780°C. Additional elements in the composition such as tin or indium can reduce the liquidus temperature even further. The use of a braze material requires that not only the die material and metallization be temperature compatible, but also the substrate material and metallization must be able to adequately withstand the temperature excursion. This stipulation constrains the number of currently available options for substrate materials and increases the risk for thermal expansion mismatches and fatigue.

Filled Glasses

Silver filled glasses are also an option when dealing with higher temperature applications. These materials have typically been used in military grade hermetic seal applications requiring seal rings and subsequent lid seal. The materials are a combination of a low melting point glasses, typically a leaded borate compositions, and a combination of silver particles and/or flake to optimize electrical and densification properties. The firing temperature can be tailored by strict control of the glass composition and adjustments as necessary to the silver flake distributions. Most commercially available silver filled glasses are fired in the range of 300°C to 500°C. The fired composition can contain up to 90% silver by weight resulting in an excellent thermal conductivity and reasonable conductivity. A downside to the

glass system is the high strength coupled with moderately high thermal expansion and an inherent brittleness of the glass.

Polymer Materials

Polymer systems made up primarily of epoxy resins currently have a wide variety of uses including electrical and thermally conductive die attach, under-fill applications, and encapsulations just to name a few. Epoxies can be divided into two primary categories: thermoplastic and thermoset. The thermoplastic epoxies are long linear polymer chains that can be reheated without producing a chemical change and reformed as many times as needed. Thermoset epoxies are polymer chains that cross link during the curing cycle resulting in an irreversible chemical reaction producing a three dimensional network [3.9]. Though many factors are important in material selection, the primary focus is the glass transition temperature (Tg). There are significant differences in critical properties including modulus and thermal expansion between the two regions. The behavior of thermoplastics and thermosets are similar below the glass transition with the modulus decreasing as temperature increases. Above Tg, the modulus will continue to decrease typically at a much faster rate for thermoplastics while the thermosets will remain constant. Thermoplastics typically have a lower glass transition point than their thermoset counterparts. One primary advantage to epoxies is the ability to absorb stresses during temperature cycles for processing, testing, or operation. The disadvantages to epoxies are related to decomposition and moisture. With higher temperatures, the polymers can begin to breakdown and outgas products into the die cavity that can result in failure. Moisture is a problem with all polymeric materials because the absorption may be slow, but it cannot be stopped. This is particularly the problem with military and space applications requiring hermiticity. One potential solution or improvement may be the use of cyanate ester resins. These resins have the ability for higher Tg, higher purity, more stability, and lower moisture absorption than typical epoxy compositions [3.10].

High-Temperature Solders

This sub-section analyzes different materials used for die attach solders. Prior to this discussion, there needs to be a brief discussion on terminology associated with phase diagrams [3.11][3.12]. Phase diagrams are separated by the number of elements present in the diagram. Most solders can be described with either a binary or ternary diagram as they typically have only two or three primary constituents. All phase diagrams are shown under equilibrium conditions and in the form of composition verses temperature. The solidus temperature is a point below which the constituents are completely crystalline and no liquid exists. The liquidus temperature is the temperature above which all components are liquids and no solid can exist. A eutectic is a point where the solidus and liquidus lines intersect. At that point, a solid changes directly and completely to a liquid without any residual solids or vice versa depending on whether the temperature is increasing or decreasing. If not at a eutectic, there exists an area between the solidus and liquidus line where both solid and liquid exist [3.11].

Gold Tin

As mentioned earlier, there are three primary solders in use today for high temperature solder applications. The first and lowest temperature solder is gold tin. With a eutectic temperature of 280°C, this material is slightly below the outlined temperature of 300°C. The typical composition of the eutectic solder is 80/20 AuSn [3.12]. The typical soldering profile would exceed the liquidus or eutectic by 30-50°C and remain there for a short time to reduce the formation of intermetallics. In the case of AuSn and other gold alloys, a gold metallization can be used on the mating surfaces to increase the amount of gold in the alloy through diffusion. This gold would be thicker than a typical immersion deposit used for oxidation protection. The time for joint formation and possibly also the temperature would increase in order to ensure the diffusion of gold into the joint. An analysis of the phase diagram shows that the slope of the liquidus line is rather steep resulting in significantly higher temperatures with small decreases in tin concentration. As can be seen, there are a number of phases that can exists with less tin concentration. Overall, the material is naturally less stable than the eutectic composition, and the

increase in intermetallics changes the bulk properties of the solder. This could result in induced stress, increased brittleness, and changes in thermal expansion that could negatively impact reliability. With the use of this material, special care must be taken to eliminate any tin components that might be included in the design such as typical surface mount capacitors. The gold tin diagram is relatively complex due to several potential phases and solid solutions that can form. Just as gold can diffuse into the system, tin will shift the composition to a point where a eutectic could form as low as 209°C at 10/90 AuSn.

Gold Germanium and Gold Silicon
Similar to gold tin, these products are simple binary eutectic alloys [3.12]. In both cases, the eutectic temperature is around 363°C for a composition of 88/12 AuGe and 98/2 AuSi; thus, it is only necessary to analyze one phase diagram. In the case of gold silicon, several different approaches are utilized to achieve this composition with typical silicon based die. With the aid of diffusion, a pure gold or 99/1 AuSi perform can be used in place of the traditional eutectic to reduce cost, simplify processing, and reduce excess silicon in the joint. During the reflow profile, the die is agitated manually or with increased pressure while the solder is molten to increase the diffusion reactivity and promote wetting. Due to the simple nature of both of these compositions, no additional phases appear to be present in the diagram. This results in a mechanical verses metallurgical bond between the single eutectic composition and pure metal rich areas. Compared with gold tin, increasing temperature by means of diffusion is more difficult and could have significantly detrimental results.

Gold Indium
Currently, there is limited availability for gold indium solders due to the mechanical properties and general alloy characteristics. Typically, indium has been used on traditional lead tin alloys to improve the ductility and suppress the melting point. From an analysis of the phase diagram [3.12], the melting point of pure indium metal is about 156°C. The current alloy composition is 88/12 AuIn that has a liquidus and solidus point of 485°C and 451°C, respectively. There is currently little data available to assist in characterizing this alloy among the other options, but based on temperature alone, it presents some merits of interest. The other interesting aspect of the AuIn system is the presence of the AuIn and $AuIn_2$ compositions with a eutectic point of 495°C. A composition containing only 58% gold would be advantageous from a cost perspective as well as theoretically having an increased ductility. The downside to most indium alloys is corrosion resistance though the gold combination could result in sufficient properties depending on the environment. Naturally, the composition described above is not the most stable version of the system; therefore, further investigation and testing would have to be employed to determine the practicality. As with gold tin, there are several phases that exist or coexist within this system opening up the possibility for further diffusion processes to increase joint temperature.

Braze Alloys
As mentioned earlier, braze compounds have been around the electronics industry for some time finding uses with high temperature ceramic packages. Most of these packages are alumina based with initial firing temperatures above 1500°C with excellent mechanical and thermal cycling characteristics. As technology advances, more materials are targeted for high thermal dissipation in high power applications and low dielectric constant and loss in high frequency applications. These materials are typically lower temperature materials, 850°C to 1200°C, which may not possess the mechanical and/or thermal capabilities of HTCC packages. The alloy selection must also reflect this potentially reduced temperature cycle and pay consideration to mechanical properties. Braze alloys are supplied under a variety of names by a variety of manufacturers though the most common may be Wesgo Metals and Johnson Matthey. Most braze alloys are based on precious metals including gold, silver and platinum; the cost of which must also be a consideration.

Silver Copper Systems
The traditional system for ceramic packaging as mentioned earlier is the silver copper eutectic [3.12] or Cusil® [3.8] formulation at 72/28 AgCu and a eutectic of 780°C. Depending on the substrate material,

the required brazing temperature of 830°C or higher can exceed the practical limits of the ceramic materials or metallization especially in glass ceramics.

This composition provides the starting point for braze materials with melting temperatures between 600°C and the eutectic point. These brazes incorporate the copper silver composition with a third element to suppress the melting point. These materials, as in the solders, are typically indium and tin. These products contain 60 to 70% silver, 25-30% copper, and 5-15% of indium or tin [3.8]. Due to the complexity of the phase diagram, these compositions will not be discussed thermodynamically, but review of a ternary diagram will show formation of multiple solid and liquid phases in these composition ranges depending on the isothermal section. All of these compositions have very high mechanical strength and thermal expansions similar to the bulk metals. These values are directly compared in a later sub-section.

Other Silver Alloys

For completeness, two other braze alloys could be of interest in SiC applications. These alloys are not very common in the current environment, so little information can be obtained relating to materials properties. The two alloys are 90/10 AgGe and 95/5 AgAl [3.8]. Upon examination of their phase diagrams [3.12], the eutectic point of AgGe is closer to 82% silver by composition resulting in a 651°C eutectic. The differences in composition may be related to process capability as a solid solution of silver is observed. As produced, the 90/10 AgGe composition has a liquidus temperature of 790°C and a corresponding solidus of 651°C. The temperature of the 95/5 AgAl is higher than the other materials discussed thus far having a liquidus of 830°C and a solidus of 780°C.

Active Metal Brazing

In the process of active metal brazing, a non-metallized ceramic is joined directly to a metal with the use of a filler metal that has elemental precursors to promote wetting and chemical reactions to the ceramic substrate. Most alloys use titanium as the precursor element in the alloy. The titanium reacts directly with the substrate materials forming multiphase components at the surface. The reaction products depend on the nature of the base ceramic materials whether they are oxide, nitride, or carbide based. Active braze alloys [3.8] are available in common compositions described earlier including silver copper and silver copper indium. Due to the nature of the process and composition changes due to the titanium, these alloys have a slightly higher liquidus temperature than their non-active counter parts.

Filled Glasses

Silver filled glasses have been used in military and aerospace packaging for die attach material, lid seal, and variety of related hermetic applications. As mentioned earlier, the glasses are fired at temperatures between 300°C and 500°C depending on the composition and loading. After firing, the die attach material is a matrix of silver embedded in a glass matrix developing a primary advantage in high thermal conductivity and good electrical conductivity. Just as with the solders, the glass composition follows a phase diagram, but it will not be discussed in detail due to complexity. The typical formulation is centered on a lead borate composition [3.6]. One major problem with the use of glass die attach is the need for firing in air to drive the oxide reaction to metal surfaces. The firing process is also very tedious due to number of phases and compositions that can form in the firing region. The ramp rates must be well monitored, and the time at temperature must be sufficient to promote adhesion. For this reason, materials properties will be discussed later as they pertain to comparison with other methods, but no further discussion is merited at this time.

Filled glasses can also include thick film paste compositions. Some of these compositions have been designed for lower temperature brazing applications, specifically for use with glass ceramic materials or low temperature cofired ceramics (LTCC). This topic is not addressed further since it can be very product specific.

Polymer Adhesives
For the most part, polymers do not perform well at elevated temperatures because of breakdown in the molecular structure. The modulus of the material can decrease by an order of magnitude over a very short temperature range, and the thermal expansion is typically very high and can increase by 2 to 10 times above the Tg. Though the modulus can change significantly, this very property affords these materials elasticity and forgiveness under stress. For this reason, adequate polymeric materials will continue to be sought to fill the gap. Another concern especially for high volume applications is the time required for epoxy cure. This is particularly a concern for higher glass transition temperatures as longer times and higher temperatures are needed. Thermal conductivity for polymer materials is also low compared to the other alternative discussed.

In order to be effective, the polymer should have a high glass transition temperature (Tg). The Tg of typical high-temperature polymers is 180°C, but the area of interest in this case is defined at or above 300°C. Some of these polymers are still utilized for high temperature applications. This is the case for a common epoxy material P-1011 manufactured by Epoxy Technology [3.13]. This material has the capability of continuous operating temperatures to 350°C while still having a relatively low transition temperature. Another material of interest is E3084 also manufactured by Epoxy Technology [3.13]. This material boasts glass transition temperatures greater than 300°C under selected cure conditions at higher temperatures but similar times. It has a comparable thermal expansion to its counterpart below Tg, increased thermal conductivity, and higher die shear. Recently, cyanate ester resins have been investigated to replace or augment the traditional epoxy resin particularly for high temperature applications. Some commercially available materials include Ablestik JM7000 and Loctite QMI 301 [3.13]. These resins typically have a glass transition in the 240°C to 270°C range with good thermal stability up to 360°C. These materials typically have very high purity couple with low moisture absorption. All of these materials have thermal expansion coefficients below the glass transition temperature above 33 ppm/°C which is roughly double that of metallic solders and glasses. Above the glass transition, the values are as high as 115 ppm/°C. Further properties comparisons will be made in the next sub-section.

Material Comparison
Several potential solutions have been discussed as they relate to individual families of materials. In order to get a better view of these materials, expanded physical property data will be compared side by side for the materials discussed above. This will help gain a better understanding of some of the actual trade-offs that occur when choosing a material. The information provided is manufacturers reported data; thus, this data is subject to individual test methods, setup, and reporting. This data is used only as a reference for broad comparison of traditional physical properties.

The data in Table 3.2 [3.13] is arranged by order of increasing temperature to show the varying levels discussed. The values for traditional 63/37 SnPb and 95/5 PbSn have been included to reference and benchmark various alternatives.

As can be seen from Chart 1, solutions for most every temperature range can be found though there is a bit of a dead area in the 500°C -600°C range. As expected there is interleaving of the solder, glasses, and epoxies in the near 300°C temperature range, but the distinction of braze alloys by processing temperature is severely reinforced. A natural assumption based on the compositions described might be to attempt to create higher level alloys with the AuSn or AuGe solders as in the silver bearing brazes. One possible approach might be diffusion bonding with a dissimilar metal as in the case of titanium additions to active braze alloys. A deep understanding of the resulting system must be obtained prior to any experimentation as reduced temperature phases or solid solutions may form instead. The general nature of the polymer components is described using the glass transition temperature rather than the defined continuous exposure temperature. This can be a bit misleading but is a result of the nature of the reported properties.

Table 3.2 Die attach physical properties.

Bulk Physical Properties	Density	Temperature Liquidus or Tg	Thermal Expansion	Thermal Conductivity	Tensile Strength	Young's Modulus	Shear Strength
	g/cc	°C	ppm/°C	W/m-K	MPa	GPa	psi
P-1011	3.19	180	37	1.29			700
SnPb (63/37)	8.4	183	25	50	51.7		6200
QMI 301 *	3.8	240	45	1.9		6.9	600
JM7000		240	36	1	17	10	
AuSn (80/20)	14.51	280	16	57	276		40000
E3084 * **	3.2	300	42	2		1.4	3400
PbSn (95/5)	11.06	312	30	23	27.6		2100
AuGe (88/12)	14.67	356	13	44	185		26825
Silver Glass		420	16	80		11.5	
AuIn (82/18)	14.9	485					
AgCuIn (61.5/24/14.5)	9.8	705	18.5	55	448	76	
AgCuInTi (59/27.25/12.5/1.25)	9.7	715	18.2	70	455	76	
AgCuSn (60/30/10)	9.75	718		30	462		
AgCuIn (63/27/10)	9.8	730	19	85	420	81	
AgCuSn (68/27/5)	9.9	760					
AgCu (72/28)	10	780	19.6	371	372	83	
AgGe		790					
AgCuSnTi (63/34.25/1/1.75)	9.7	805	18.7	170	402	83	
AgCuTi (63/35.25/1.75)	9.8	815	18.5	180	346	83	

* Modulus at 25°C ** Modulus at 300°C = .09 Gpa

Most data sheets, epoxies in particular, contain information based on a single cure cycle which is typically not the highest temperature or time. The related data must also be evaluated in this context. Based on the reviewed material literature, the continuous use temperature can be between 300°C and 350°C for epoxies defined in this table. The data for the E3084 specifies a continuous temperature of 200°C when cured at 200°C for 1 hour. This cure schedule is used to obtain a glass transition temperature of only 225°C, so it would seem logical higher usage temperatures could be obtained when utilizing the cure cycle for 300°C glass transition. Since the use of temperature is not sufficient to select or distinguish between alloys further investigation must be performed. Due to the differences in material performance and composition, some property information is easier to obtain than others. This results in incomplete or incomparable data as can be seen with the strength properties.

Charts 2 and 3 represent significant pieces of information when making materials decisions. The tensile strength of a material is expressly the amount of tensile or pulling stresses a material can withstand without failing. The definition of failure may be disputed especially with elastic and ductile materials as is the case with most polymers and some metals such as indium.

Chart 1: Material Compositions vs. Liquidus Temperature

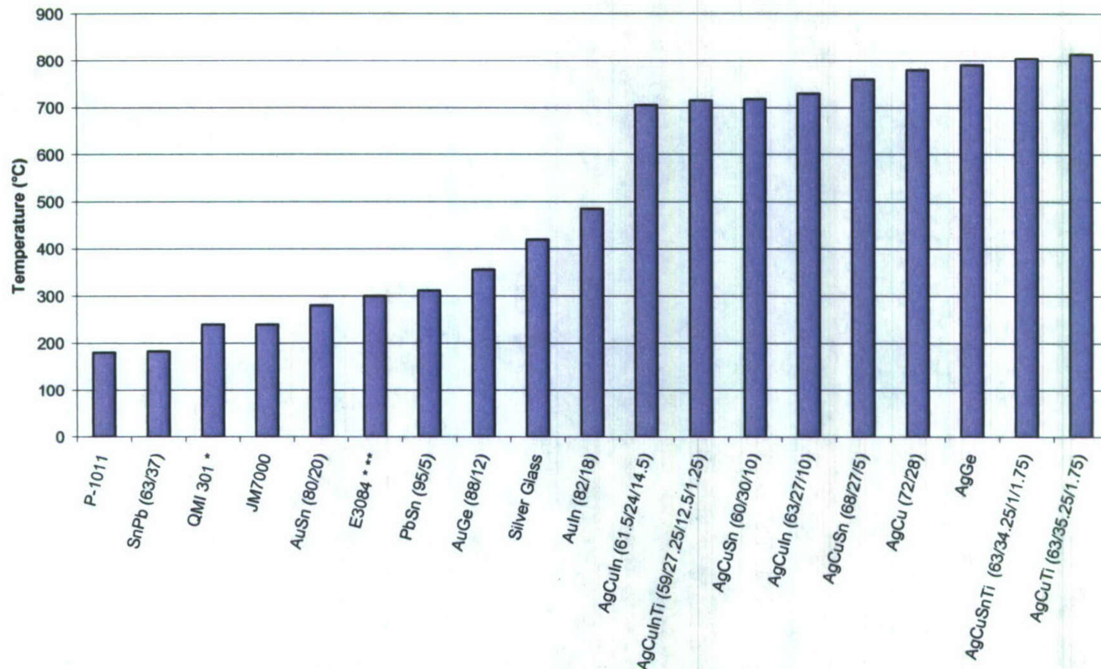

The Young's modulus is a ratio of stress to strain within a material determining how much elongation results from given stress loads. From the chart, it is readily seen that both measures result in very low values for the epoxy components as compared to alloy counterparts. These values can easily be an order of magnitude different due to the brittle nature of the alloy joints. This value has to be compared with the die and substrate values to determine what maximum values can be tolerated. The comparison of hard verses soft adhesives is also evident when comparing the epoxy and even tin lead values to that of the hard solders and even harder brazes.

It is also worth noting that the strength of gold tin is higher than that of the higher melting point gold germanium. Though no information was available, a similar behavior may exists with the silver germanium braze alloy. To compound the issue, the amount of elongation that the joints are exposed to for the strength measurements is dependent on the thermal expansion of the constituent materials involved. The ceramic values listed earlier were all below 10 ppm/°C.

The thermal expansion values are not independent of the strength of the material. Thermal expansion mismatches between the die, attach material, and substrate become evident as the materials begin to contract during cool down. More expansion mismatch results in more stresses built up leading to one of the materials yielding to the others. This may be evident in a variety of forms including die cracking, camber, metallization failure on either the die or the substrate, or attachment failure. Based on Chart 3, the hard solders and brazes appear to have a slight advantage in expansion over the traditional soft solders, and values of approximately half that of the included polymers. Since epoxies have a higher thermal expansion and lower modulus, they reach their yield point sooner than do alternative methods. This can present an opportunity for failure by mechanical means. With alloys, the thermal expansion below the solidus point is critical to the design. As the alloy begins to solidify, the alloy begins to gain strength and induces stresses into the joint.

Chart 2: Composition vs. Strength

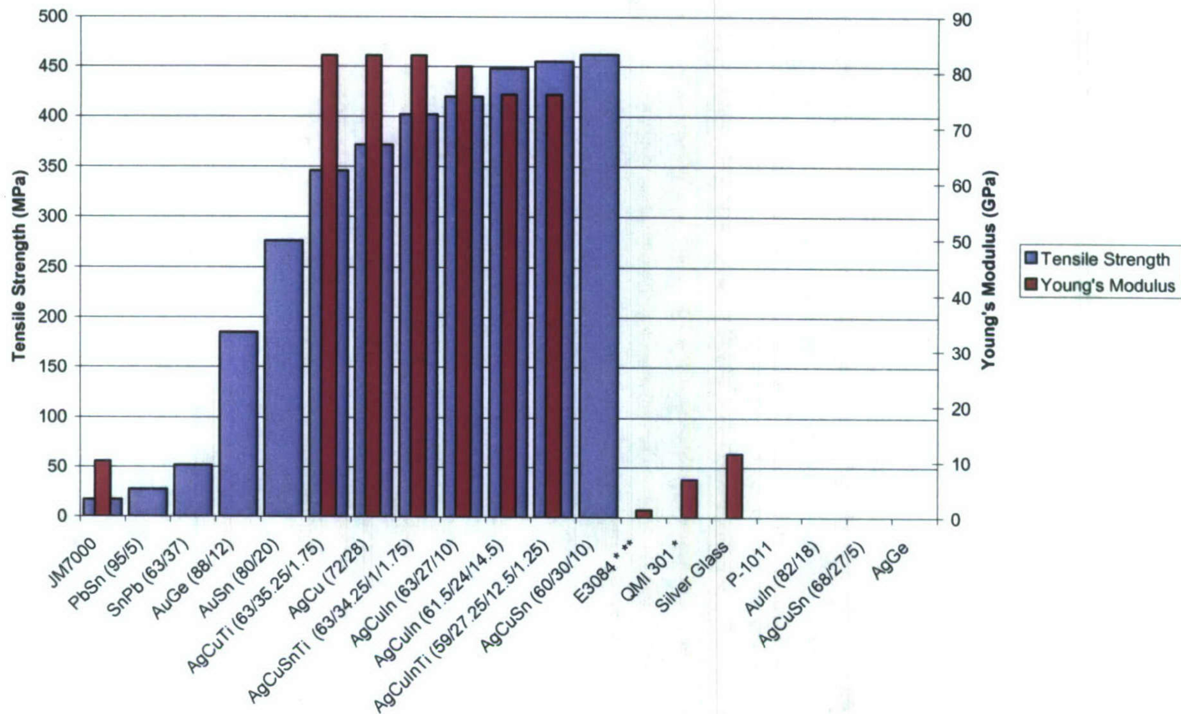

For most substrate materials shown in Table 3.1, the Young's modulus is considerably higher than that of the alloy which could result in bond line cracking. This failure may or may not be catastrophic. Problems of this nature must be solved in research as it presents a significant problem in a production environment. Reliability testing is crucial for non-catastrophic defects since cycling and fatigue will exacerbate the problem. Other non-destructive options exist though processes such as acoustic microscopy may be difficult with complex alloy structures having a number of different phases with different densities. The last comparison is thermal conductivity. Though mechanical integrity is the primary concern, thermal performance can destroy a package just as quickly. Increased operating temperatures result not only in increased heat storage but heat transfer. For example, a die is operating continuously at 300°C ambient conditions while processing high power applications. The nature of the applications are not efficient and could produce significant additional heat flux resulting in very high die temperatures concentrated at the die interface to the substrate and heat sink. Some of the solder applications have thermal conductivities rivaling the best substrate materials. This could allow more efficient heat transfer through the interface limiting isolated hot spots on a die.

Conclusions

A variety of die attach materials have been presented dealing directly with classification, general properties, and specific products. The choice of a die attach materials for applications above 300°C is rather complex. Some of the materials addressed in this work require significant research and experimentation to determine ultimate suitability. The balance of mechanical and thermal attributes will never be ideal because the properties that make a good die material, die attach material, and substrate are vastly different in chemistry and crystalline structure just to name a few. Each material has distinct functions, and independent of the material selected, the die attach material must act as the stress relief between the die and substrate while providing adequate thermal and electrical performance.

Chart 3: Composition vs. Thermal Expansion

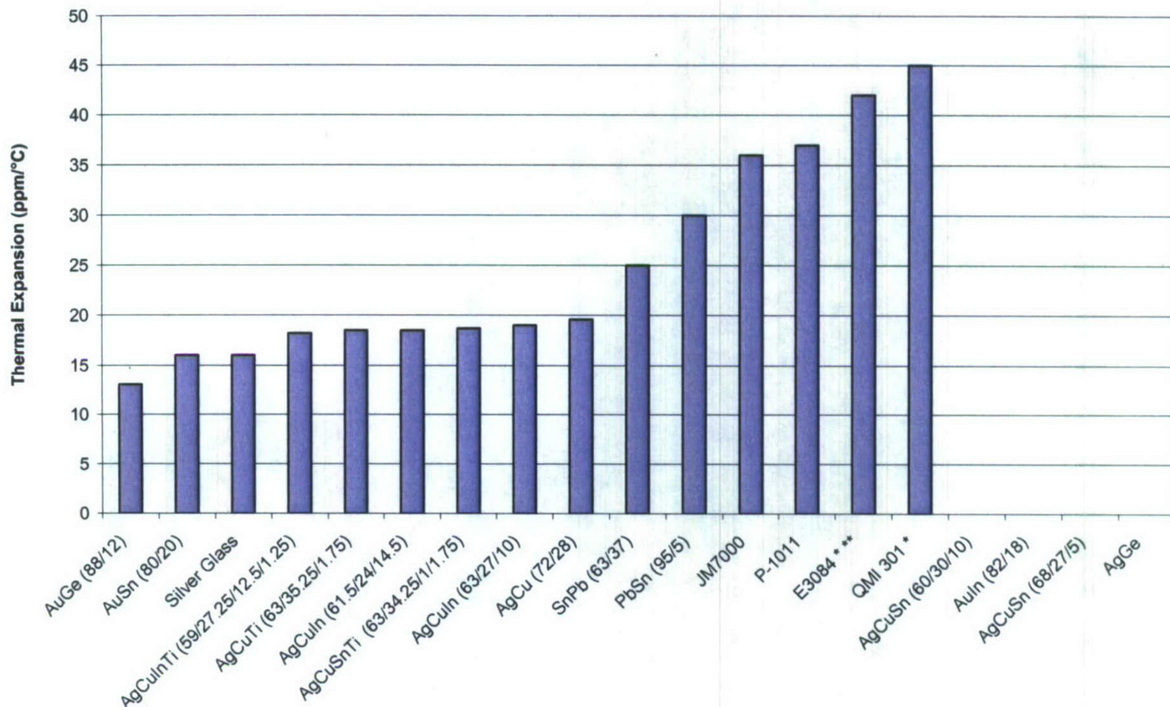

Typically, epoxies are preferred for material cost and stress relief but suffer in decomposition and thermal properties. Alloys present a renewed challenge with higher temperature materials and environments, but the cost of using gold, silver, or platinum will continue to remain an issue. The reaction bonding approach of current high temperature alloys such as AuSn or AuIn also presents unique options for achieving a higher melting point thermally stable alloy by the controlled addition of the base metal into the soldering process. The reflow temperatures for reaction bonded approaches can achieve greater than 300°C stabilities with the addition of plated base metals, but in addition to the added expense, the mechanical properties can be significant compromise as the alloy strength and brittleness will typically increase.

The primary reason for inclusion of active metal brazing is not to promote direct bonding to a ceramic substrate which does not relate to die attachment but to correlate the metallurgical aspect of the active braze to integration with SiC devices. A method of manufacturing SiC devices results in the use of titanium as part of the metallization scheme. The titanium reacts with the silicon carbide during annealing much like the active braze behavior. The addition of titanium into the alloy system also results in an increase in temperature. One option might be the use of a standard silver copper braze in the direct presence of the titanium metallization. Under this premise, the titanium would bond by means of diffusion with the braze alloy resulting in a strong bond comparable to that of active brazing and possibly having a higher temperature than the initial braze. This could be especially useful for devices that might see up to 600°C and require further lid seal or leading applications. Further investigations would have to be made into the ternary or quaternary systems that develop to ensure proper chemical behavior at the projected alloy.

Sub-task 3.3: Spray-Cooled Power Conversion Modules

This sub-task was performed by Mr. Brian Rowden as part of his doctoral work. Mr. Rowden was initially supervised by Dr. Fred Barlow. Dr. Balda also provided technical support on the circuit topology of the PCM.

Introduction

It is well know that it continues to be very difficult to get bare die of SiC devices since most devices are still in their developmental stages. Most of the work is being funded through DARPA projects so most devices are used by researchers directly involved in these DARPA projects. Faced with the difficulties of obtaining bare die of SiC devices, the researchers decided to focus on the integration and packaging of the spray-cooled thermal management solution with a PCM envisioned under the "all-electric ship" concept. Fig. 3.11 shows a block diagram of a bi-directional PCM consisting of a dc-ac H bridge, a high-frequency transformer (HF-XFMR) and an ac-dc H bridge. This modular PCM could be part of a PCM4, an isolated PCM having three-phase voltages on one side (i.e., 4.16 kV) and a dc voltage on the other side (i.e., 1 kV).

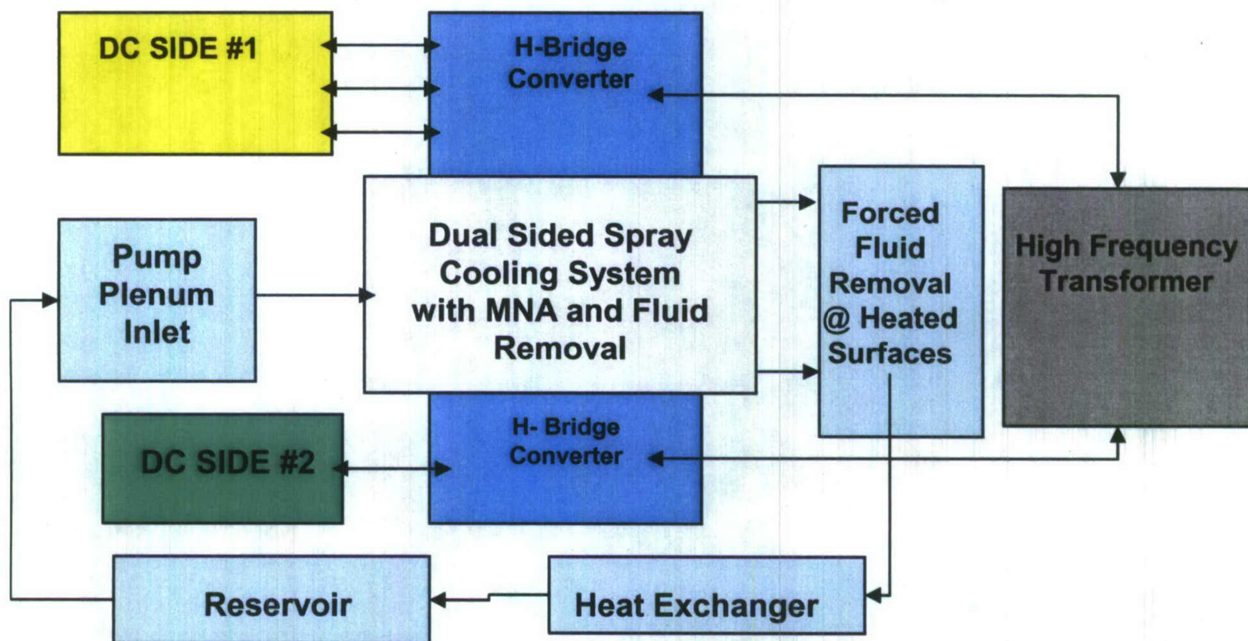

Fig. 3.11 Block diagram of a spray-cooled PCM.

The figure shows one dc side (yellow block), the H-bridge converter (blue block on the top), the HF-XFMR and the second H-bridge converter (blue block on the bottom). The core of the HF-XMFR could be built using nanocrystalline materials in addition to high density copper foil windings as compared with the traditional ferrite and Litz wire structures to provide an order of magnitude increase in power density.

System Description

Fig. 3.12 illustrates a graphical view of the complete PCM system integration and packaging designed for this scaled-down PCM. An exploded view is provided in Fig. 3.13 to illustrate the internal construction of the spray-cooling system. The main spray cooling concept is to use a common plenum to supply two multiple-nozzle arrays, each one used to cool a power converter in order to increase power density and to demonstrate a vertical packaging approach. Both converters utilized for this experiment are H-bridge converters. The top of the figure shows the gate drivers and control circuitry (labeled #1 in the figure).

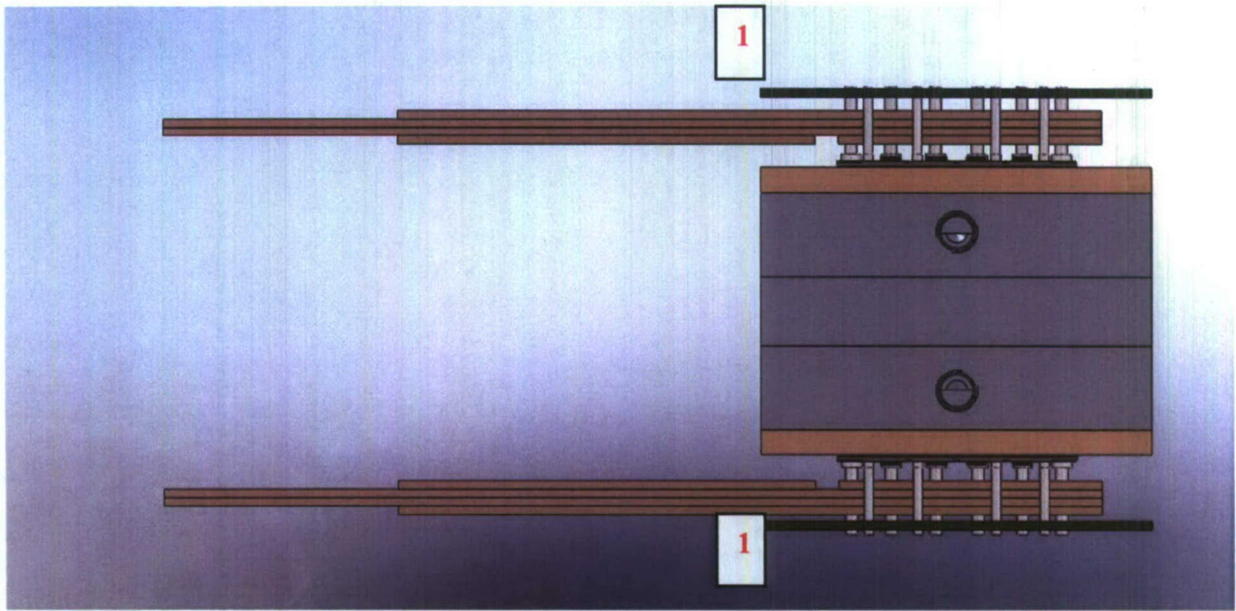

Fig. 3.12 Graphical view of the complete PCM with drive circuits and bus bar interconnect.

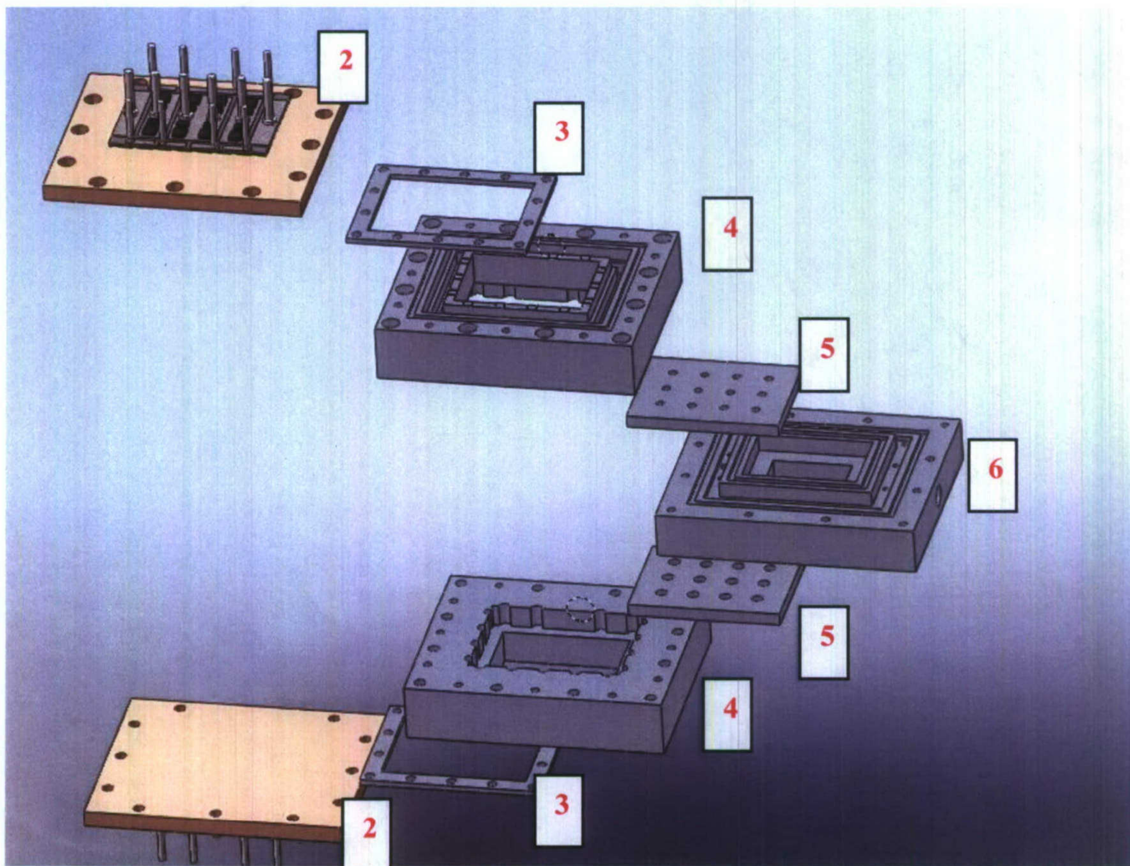

Fig. 3.13 Integration of a sprayed-cooled thermal management solution with a power converter.

The components are surface mounted, and the switching frequency range is 5 to 20 kHz due to limitations of the IGBT available in bare die form. The control board also contains the individual power supplies necessary for the gate drive signals integrated at the board level so a single 120 Vac signal is all that is required for the drive circuitry. Below this board, a four layer copper bus bar is utilized for connecting to the outputs to the HF transformer, and inputs for the dc bus on converter 1, and inputs from the HF transformer and outputs to the load on converter 2. The power devices are packaged on nickel plated AlN DBC (Direct-Bond Copper) with surface mount power and gate pin connections to interconnect with both the bus bar and the gate driver board as labeled #2. The distance required to fully develop the spray pattern is 0.375" and is established between the sprayed base plate of the power module and the multiple-nozzle array by the forced fluid removal module labeled #4. An insert is utilized for fluid management in the removal system labeled #3 in the figure. The nozzle array consisting of 3x4 nozzles has been labeled #5. Lastly, label #6 corresponds to the common plenum providing the reservoir for fluid being sprayed on both sides in addition to providing additional internal common fluid removal ports. In this case, the system integration is symmetrical with respect to each power converter though different configurations could be utilized with special consideration taken for fluid balance in the plenum to ensure proper pressure development to both sides. This approach should lead to higher power densities for PCM. A cross sectional view of the spay box is shown in Fig.3.14 to illustrate the fluid flow path as well as an internal view of the fluid removal system. All of the forced fluid removal ports are connected together prior to entering the fluid removal pumping loop so the balance between the heated surface removal ports and the internal removal ports can impact the performance of the cooling system.

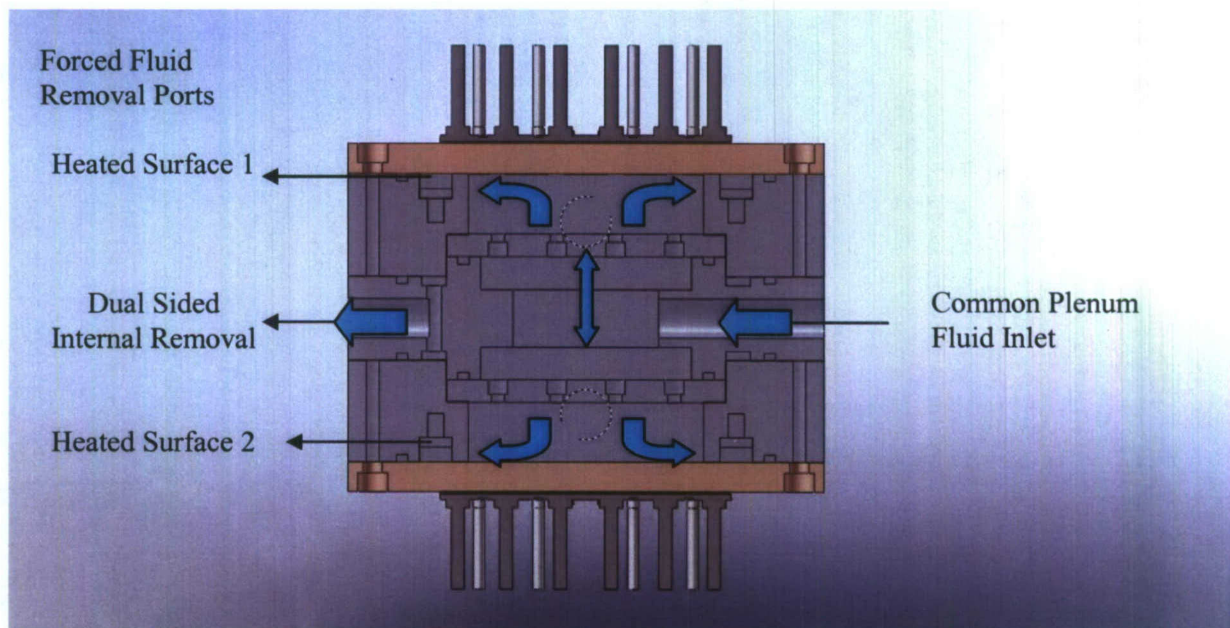

Fig. 3.14 Cross sectional view of the complete PCM.

Experimental Results

The double sided spray cooler was designed around spraying large area formats suitable for typical power electronic designs including multiple switch positions and larger power devices. The direct spray area form each side of this design is approximately 10 cm^2 with additional indirect cooling area associated with the fluid removal channels. The nozzle plate for the double-sided spray cooler was

designed to provide minimal spray overlap of the nozzles to minimize the number of interaction zones as shown in Fig. 3.15 at pressures below 40 psi. The spray pattern for the multiple-nozzle array is shown in Fig. 3.16 at 40 psi inlet nozzle pressure and significant burn-in time to ensure that the system was not building up fluid long term. The spray pattern shows minimal distortion due to the forced fluid removal as well as smooth flow patterns into the forced fluid removal channels.

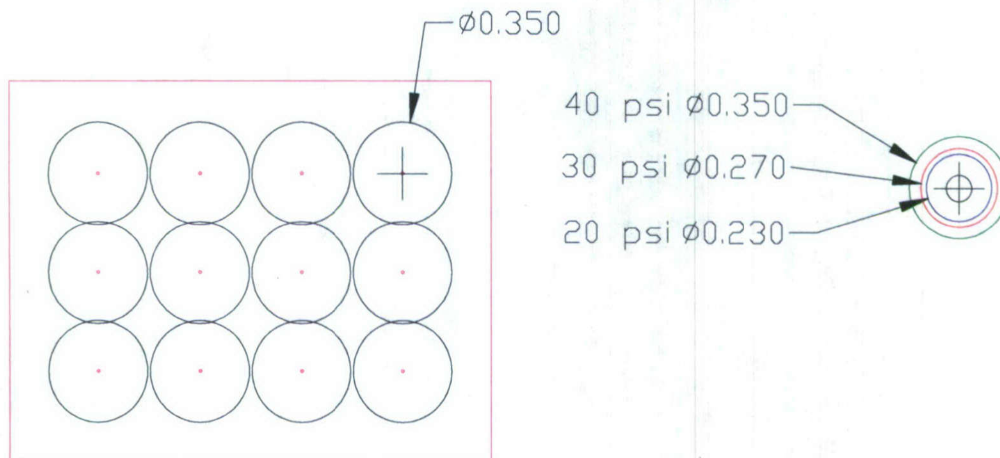

Fig. 3.15 Nozzle plate drawing showing spray pattern overlap design for 40 psi inlet pressure.

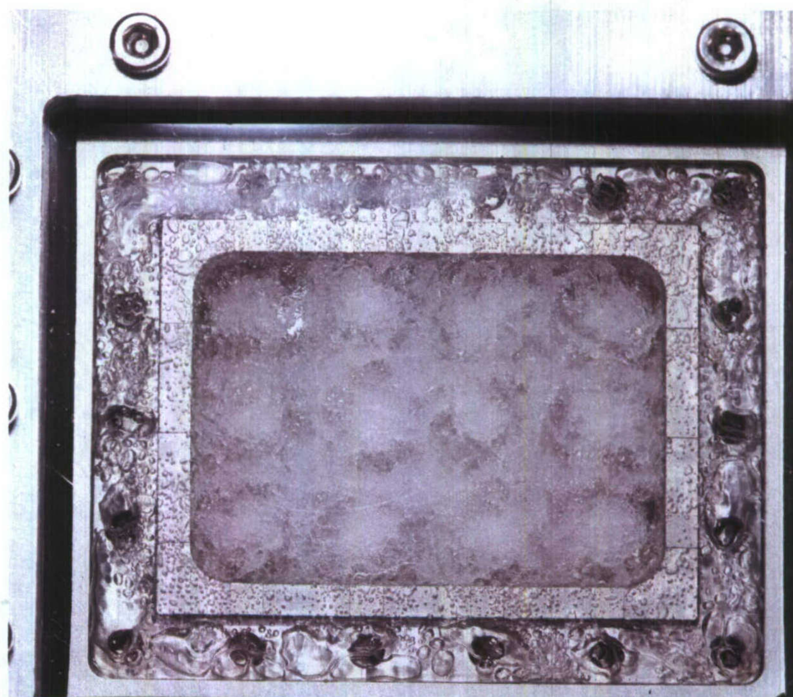

Fig. 3.16 Nozzle spray pattern at 40 psi nozzle inlet pressure and forced fluid removal.

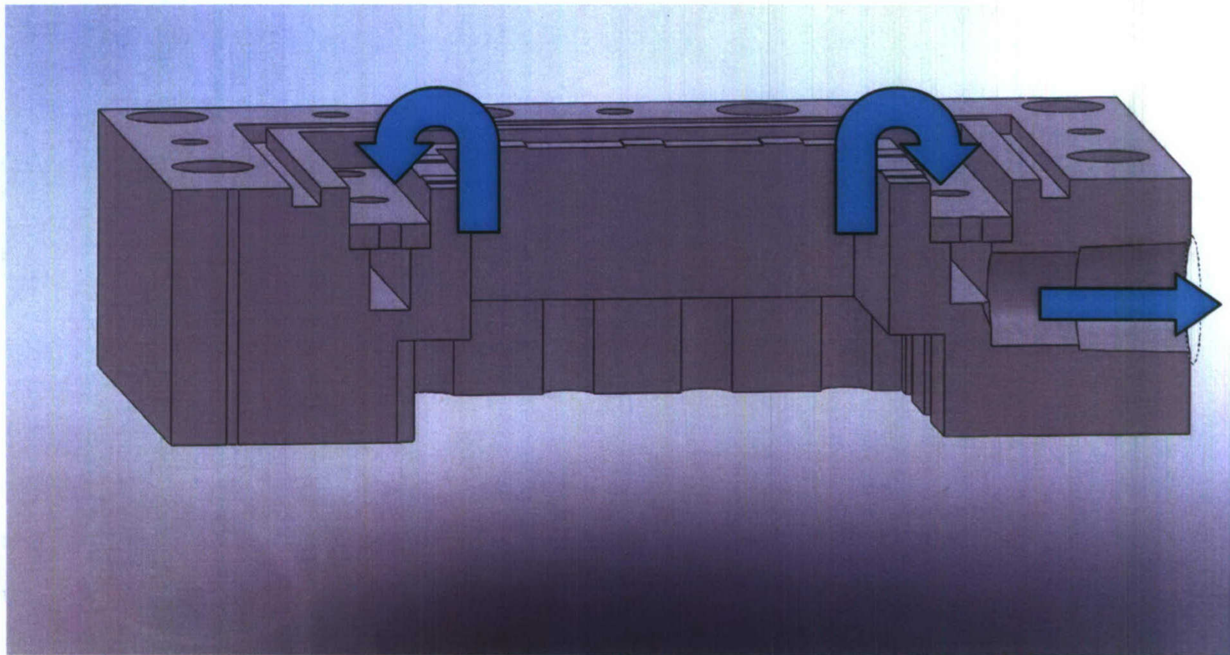

Fig. 3.17 External forced fluid removal cross sectional detailed view.

In order to manage the fluid in the confined spray closed loop system, an external fluid removal system was incorporated into the spray box at the spray surface. The fluid removal areas were created using a 0.005" – 0.010" channel gap between the active heater area and the fluid removal channel. Due to the large area, the fluid removal area was segmented to disperse the pressure differential so as to not distort the spray pattern at the heated surface. Additional fluid removal was incorporated in the common plenum area to account for backsplash, condensation, and heater surface removal inefficiency that would result in fluid congregating around the nozzle plate. These removal areas are shown in detail in Fig.3.17.

The test bench designed for this evaporator is shown in Fig. 3.18 and a schematic layout is shown in Fig 3.19 including a magnetic gear nozzle pump supplying the inlet pressure, 3-kW tube and fin forced air heat exchanger, magnetic gear removal pump for the forced fluid removal system, measurement points, and reservoir. The pressure in the reservoir was measured to determine the saturation temperature of the working fluid during the testing intervals. The double sided spray cooler was thermally tested utilizing a copper block test heater on each side as shown in Fig. 3.20 with 5 individual 400-W test heaters controlled by a PID controller and power relay. The exposed copper block was completely wrapped in approximately 6 layers of alumina silicate thermal wrap for minimization of lateral thermal losses with a Kapton tape outer shell for ease of handling. The heat flux was measured using steady state 1 dimensional heat flux calculations using temperature measurements from multiple planes of T-type thermocouples. The thermocouples and measurement devices were directly wired into an Agilent 34901A 20 channel multiplexer in an Agilent 34970A data acquisition unit, and data was recorded on 10 second intervals comparing to both an external RTD as well as an internal junction on the multiplexer.

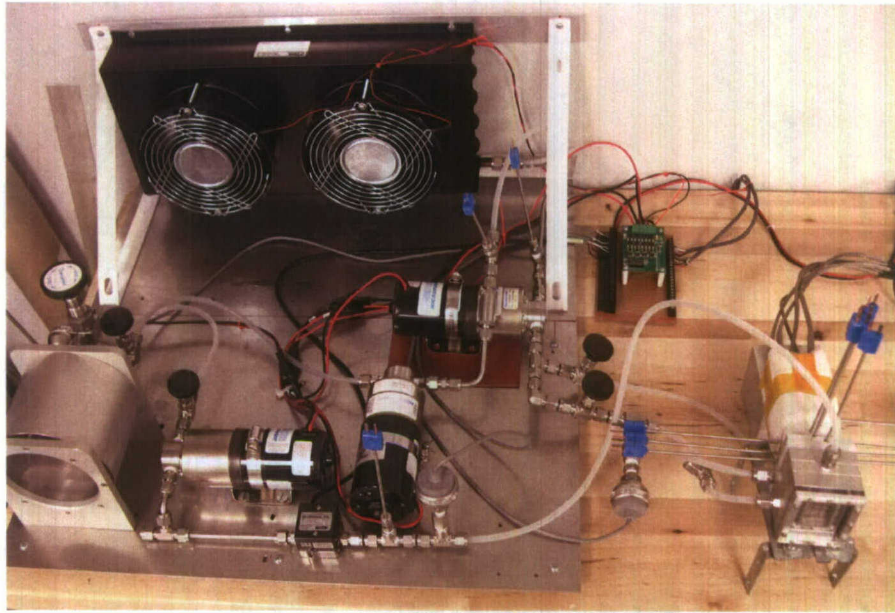

Fig. 3.18 Spray cooling test bench for double-sided evaporator.

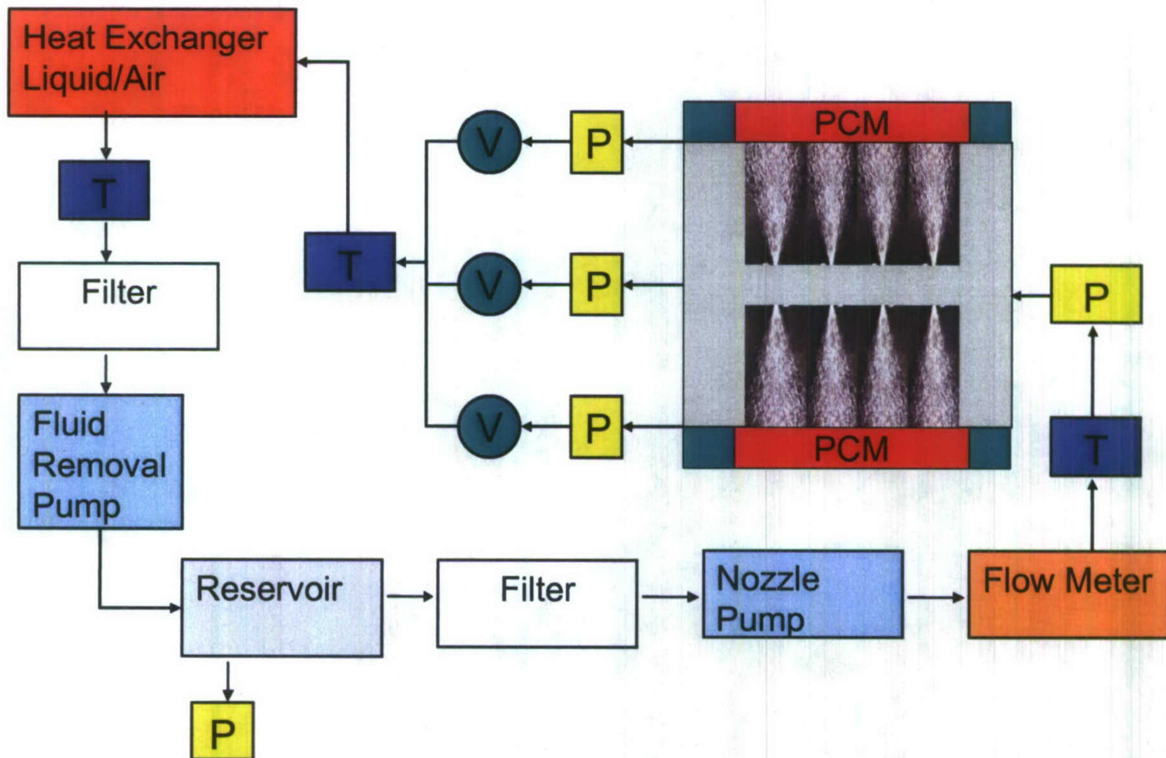

Fig 3.19 Schematic of double-sided spray cooling system.

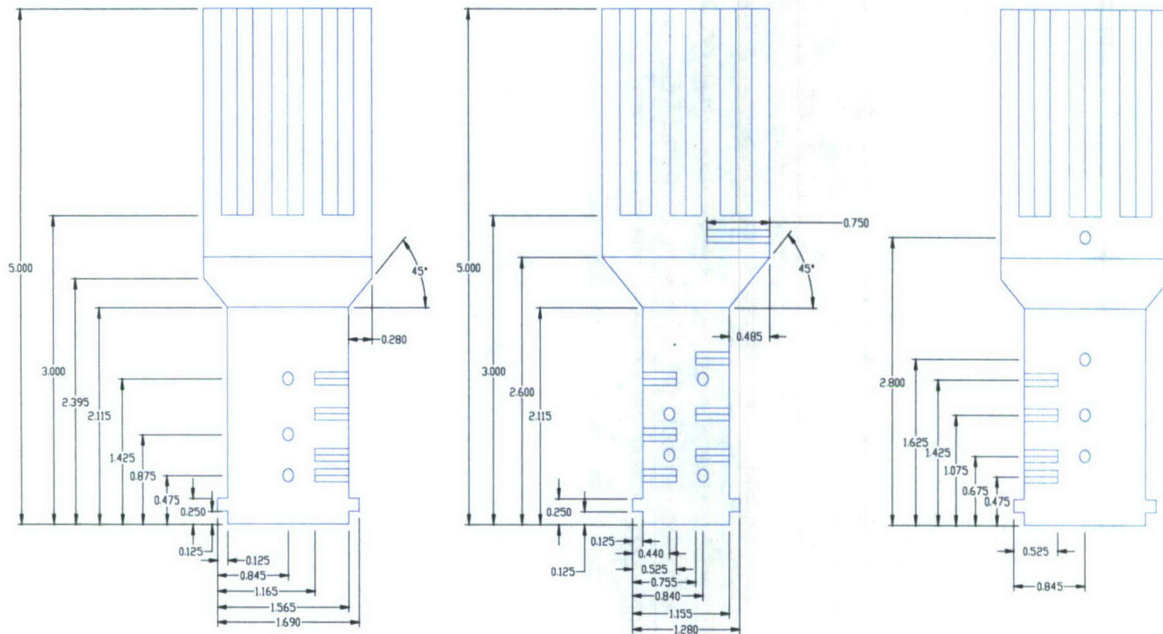

Fig. 3.20 Details of the copper block thermal test heater.

Data was taken under several conditions to determine the impact of orientation of the double-sided evaporator as well as varying inlet pressures and forced fluid removal settings. This data is shown in Fig. 3.21 to Fig. 3.22 for single-sided operation as well as dual-sided operation in both horizontal and vertical positions with the copper block test heater. The data is consistently between 50 and 60 W/cm^2 using FC-72 for the large surface area for both the single- and double-sided cooling cases with no significant differences noted between horizontal and vertical orientation. The nozzle inlet pressure was controlled at 40 psi, utilizing the voltage control of a dc motor for the gear pump, resulting in an inlet flow rate of 1.2 L/min which supplied both sides of the evaporator. It is important to note that this work was performed with using only 12 nozzles to reduce the cost and complexity for the large area, but this limits the flow rate and liquid coverage as compared to other data presented earlier in Table 2.1. This data is comparable to that of Lin et al. 2004 [3.14] which focused on 19.6 cm^2 (twice the single-sided area) but utilized 48 nozzles (twice the number utilized for a single side) to cover the spray area. Due to the modular nature of this design, the nozzle plate could be replaced with a larger array of nozzles in order to increase the spray density and available flow rate across the surface. The increased flow rate in a confined spray system comes at a price in fluid removal management in order to preserve the spray cooling concepts.

An invention was disclosed to the University officials for possible patenting.

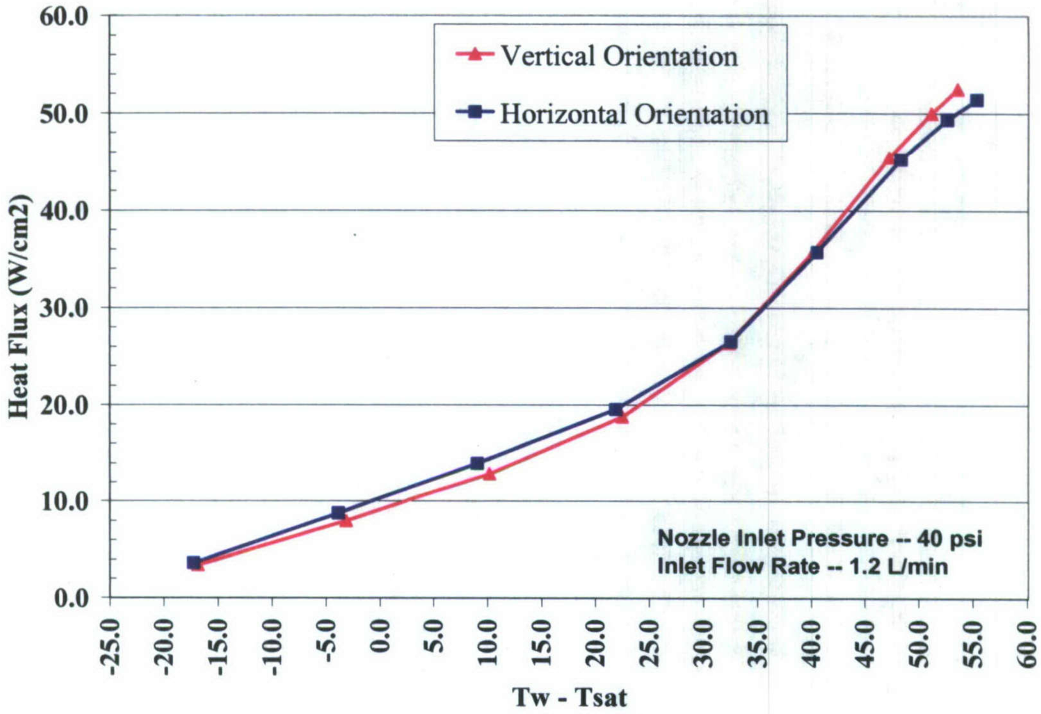

Fig. 3.21 Heat flux comparison of double sided spray box orientation.

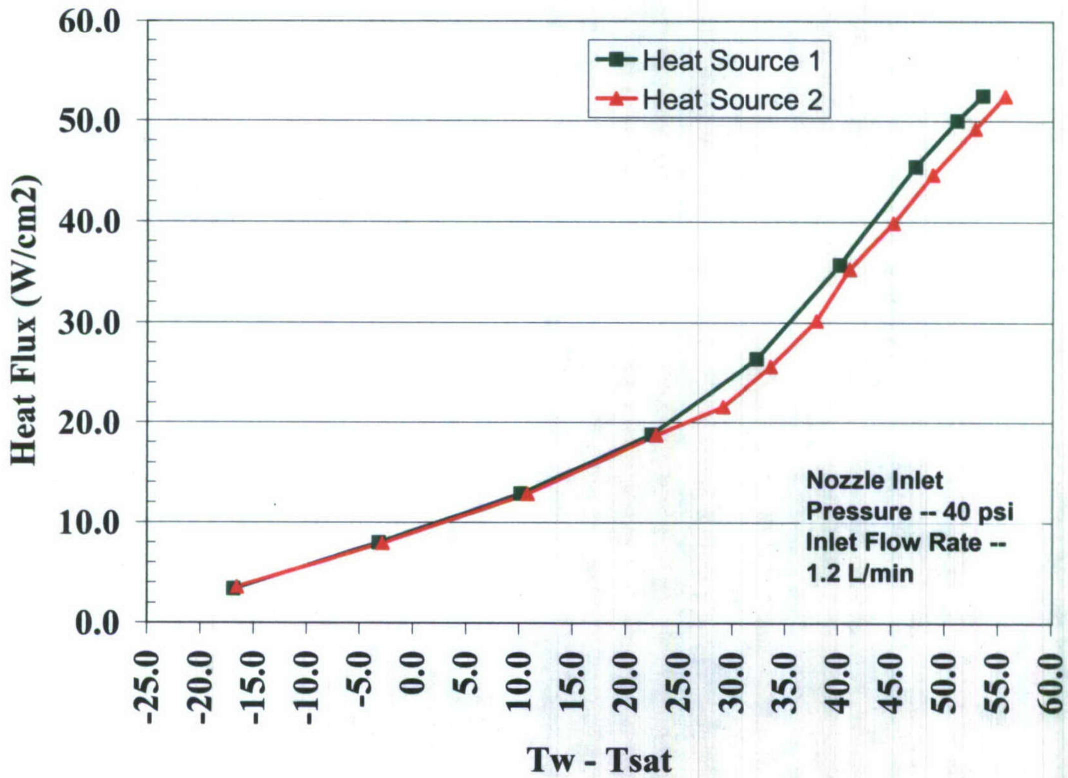

Fig. 3.22 Heat flux comparison of each side of a double sided spray system.

Conclusions

The large area double sided spray cooling system was designed specifically to accommodate traditional electronic modules that require larger sizes in order to exploit higher power levels and functionality in a single module. The double sided nature of the system provides a minimized volumetric footprint for the spray box as well as integrating complementary electronic systems, such as isolated dc-dc converters, inverter-converter systems and matrix converters, in a single 3-D vertical geometry to increase power density. The design was constructed for 10 cm^2 per side with a minimal number of nozzles to reduce cost and complexity. The forced fluid removal was integrated into the modules in an external approach complementary to the nozzle spray development though the modular nature would allow for future testing of alternate removal systems. Heat fluxes on the between 50 and 60 W/cm2 were obtained in this system with FC-72 working fluid under double sided operation in both horizontal and vertical configurations. Further optimization of the nozzle array and fluid removal system could further increase these values.

References

[3.1] F. P. McCluskey, R. Grzybowski, and T. Podlesak, High Temperature Electronics (Electronic Packaging Series), CRC Press, Inc., New York, NY, 1997.

[3.2] M.Willander and H.L. Hartnagel, High Temperature Electronics, Chapman & Hall, 1996/1997.

[3.3] P. G. Neudeck, "Progress Towards High Temperature, High Power SiC Devices", *Institute of Physics Conference Series*, Compound Semiconductors 1994, edited by H. Goronkin and U. Mishra (IOP Publishing, Bristol, United Kingdom, 1995), pp. 1-6.

[3.4] T. Martin and T. Bloom, "High temperature aluminum nitride packaging," D.B. King and F.V. Thome, *EDS*, vol. 2, June 1996, pp. P-95 to P-100.

[3.5] Bloom, T.R. (1993), "An Aluminum Nitride Package for 300ºC Operation," *Proceedings of the 1993 ECTC*, Orlando (FL), June 1993, pp. 431-435.

[3.6] Engineered Materials Handbook, vol.4 *Ceramics and Glasses*, OH:ASM International, 1991, pp. 808, 1069, 1108.

[3.7] ASM Handbook, vol.6, *Welding, Brazing, and Soldering*, OH: ASM International, 1990, page 110.

[3.8] Wesgo Metals, Alloy Selection Tables by Temperature and Physical Properties.

[3.9] Engineered Materials Handbook, vol.2 *Engineering Plastics*, OH:ASM International, 1991, page 437.

[3.10] N. Nguyen and M.B. Grosse, "Low Moisture Polymer Adhesive for Hermetic Packages", *IEEE Transactions on Components, Hybrids, and Manufacturing Technology*, vol. 15, no. 6, 1992, page 964.

[3.11] F.A. Hummel, *Introduction to Phase Equilibria in Ceramic Systems,* NY: Marcel Dekker, Inc., 1984, page 62.

[3.12] ASM Handbook, vol.3, *Alloy Phase Diagrams*, OH: ASM International, 1990.

[3.13] Data Sheet information from Epo-Tek P1011, Epo-Tek E3084, Loctitie QMI 301, Ablestik JM7000, Indium Corp. Master Solder Alloy Properties Table, Wesgo Metals Alloy Selection Tables, Johnson Matthey Alloy Selector Chart Specialised Silver Brazing Alloys.

[3.14] L. Lin, R. Ponnappan, K. Yerkes, and B. Hager, "Large Area Spray Cooling", paper: AIAA 2004-1340, 42nd AIAA Aerospace Sciences Meeting & Exhibit, Reno (NV), January 5-8, 2004.

Task 4: Technology Demonstrators

This task was led by Dr. Juan Carlos Balda who supervised the following graduate students: Mr. Joe Carr, Ananta Medury and Ranadheer Purupati. Mr. Carr is the holder of a UA Doctoral Distinguished Fellowship so the ONR contributed only $10k towards. Mr. Ananta Medury was supported by the Department of Electrical Engineering as a graduate teaching assistant (GTA). Mr. Purupati was partially supported by this ONR grant with the department supporting him as a GTA.

As mentioned earlier, the main objective of this task was developing new topologies for power conversion modules (PCM) under the "all-electric ship" concept, in particular, those PCM with heat fluxes greater than 50 W/cm^2 and a thermal management solution like spray cooling could increase the power density of the overall system leading to volumetric gains. The research team concentrated on the following:

- Sub-task 4.1: Multi-level converters
- Sub-task 4.2: Novel topology for interfacing multiple non-traditional sources to an ac power grid

This work was concurrently done with Task 3; in particular, the work in Sub-task 3.3.

<u>Sub-task 4.1: Multi-level Converters</u>

Fig. 4.1 illustrates the general topology of a PCM4, a PCM forming part of the next generation of power system for US Navy ships. The three-phase ac side has currently a voltage rating of 4.16 kV (line-to-line) and the dc side a voltage rating of 1 kV. A PCM4 subsystem consists of an ac-dc converter, a dc-ac converter, a high-frequency transformer (HF-XFMR) and an ac-dc converter [4.1]. The subset consisting of a dc-ac converter, a HF-XFMR and an ac-dc converter (marked with a red box in Fig. 4.1) could be considered as a building block.

High voltage semiconductor devices based on silicon which are suitable for 4.16 kV voltages cannot switch at switching frequencies of 10 kHz or higher which are required for volume reduction onboard ships (Si-based devices rated 6 kV can only switch at about 1 kHz). High-voltage silicon carbide (SiC) devices are still moving along their developmental stages and it is still uncertain if the current ratings required for high power applications (e.g., 1 kA) will be commercially available within the next 3 years (i.e., by the year 2011). Thus, the designer has three main options to obtain switching frequencies of 10 kHz or higher:

- Series connection of several silicon-based low-voltage semiconductor devices to satisfy the system voltage levels (e.g., 1.7 kV insulated-gate bipolar transistors or IGBT).
- Series or cascade connection of several subsystems as illustrated in Fig. 4.2.
- Multi-level converters. Hybrid topologies combining multi-level subsystems and its cascade connection are also included in this category; for example, Fig. 4.2 could realize one phase of a 4.16kVac-1kVdc PCM4 using three-level full-bridge converters and 1.7 kV IGBT enabling reaching the desired switching frequencies.

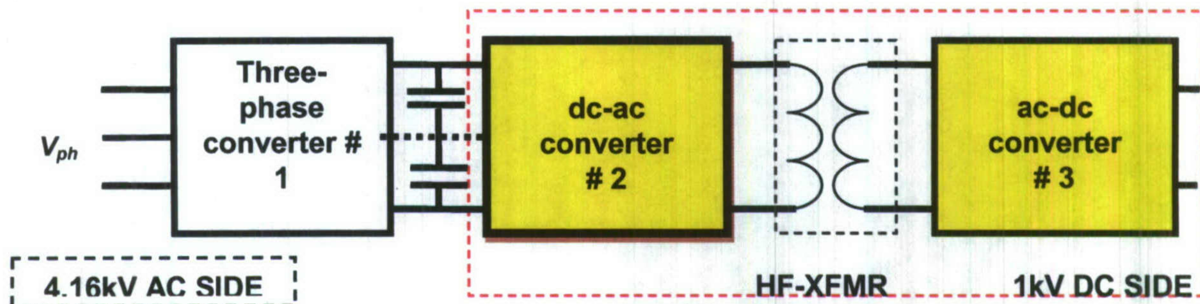

Fig. 4.1 Block diagram of a PCM4.

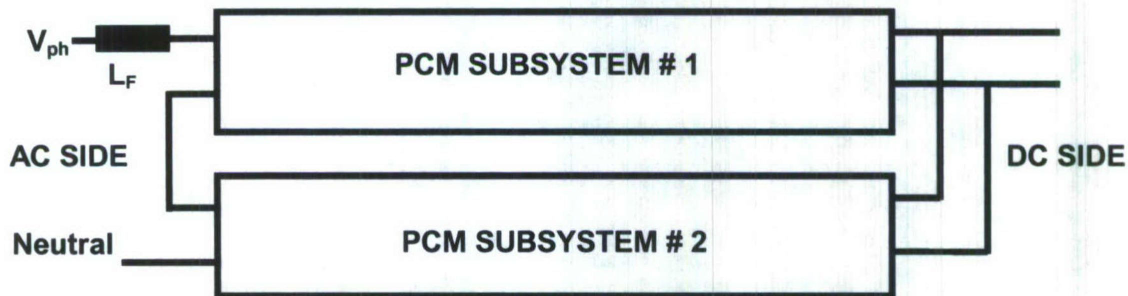

Fig. 4.2 PMC4 system rated 2.4 kV per phase on the ac side and 1 kV on the dc side.

Comparing Two-Level vs. Three-Level Converters

In general, the main advantage of using multi-level converter topologies (as opposed to using a high-voltage two-level converter topology with devices connected in series) is that the system control algorithm is simpler (with the complexity lying in the control algorithm for the subsystem). Thus, the first technical activity in this sub-task was to compare the performance of two-level (2L) converters versus three-level (3L) converters. Fig. 4.3 shows these converters representing the subsystem enclosed in the red box in Fig. 4.1 [4.2][4.3]. The ac-dc converter was realized by a diode bridge rectifier for simplicity. Fig. 4.3(a) illustrates a two-level full-bridge (FB) converter (two voltage levels can be applied to the primary side of the HF-XFMR), while Fig. 4.3(b) depicts the three-level half-bridge (HB) converter (three voltage levels can be applied to the HF-XFMR). It is noted that the number of switching devices is the same in these two converter topologies with the three-level converter requiring clamping diodes D_{C1} and D_{C2} and clamping capacitor C_{SS} beside a split dc bus. The secondary side of the HF-XFMR was not drawn in Fig. 4.3(b) because of simplicity. Zero-voltage and zero-current switching (ZVZCS) converters were selected because efficiency is important when taking into account that the electric power is generated onboard the ship is limited (i.e., there is no infinite bus to aid in power generation). References [4.2] and [4.3] as well as the master thesis of Mr. Ananta Medury (available at the Library of the University of Arkansas, Fayetteville, AR) provide detailed descriptions of the circuit design. This information is not included in this report because of simplicity, ease of reading and space.

Experimental Results

A scaled down prototype was developed for 200V input, 48V output, and 480 W for both converters to demonstrate the feasibility of the proposed ideas. The converter is a Si/SiC hybrid, utilizing SiC for the clamping and anti-parallel diodes on the primary to reduce the reverse-recovery, improve efficiency, and increase switching speed without sacrificing for high di/dt. The primary switches were International Rectifier IRG4PC30S IGBTs (600V, 16A), the anti-parallel and flying diodes were CSD10060A SiC diodes, the series capacitor C_{bo} was 1.5 uF for the two-level FB and 6.6 uF for the 3L HB, the flying

capacitor C_{ss} for the 3L HB was a 3.3 uF polypropylene capacitor, and the rectifier and series diodes were HFA25TB60 Si diodes. Table 4.1 summarizes relevant parameters of the experiment.

Fig. 4.4 displays main operating waveforms of the two converters; namely, two gate control signals, the primary current, and the bridge output voltage V_{AB}.

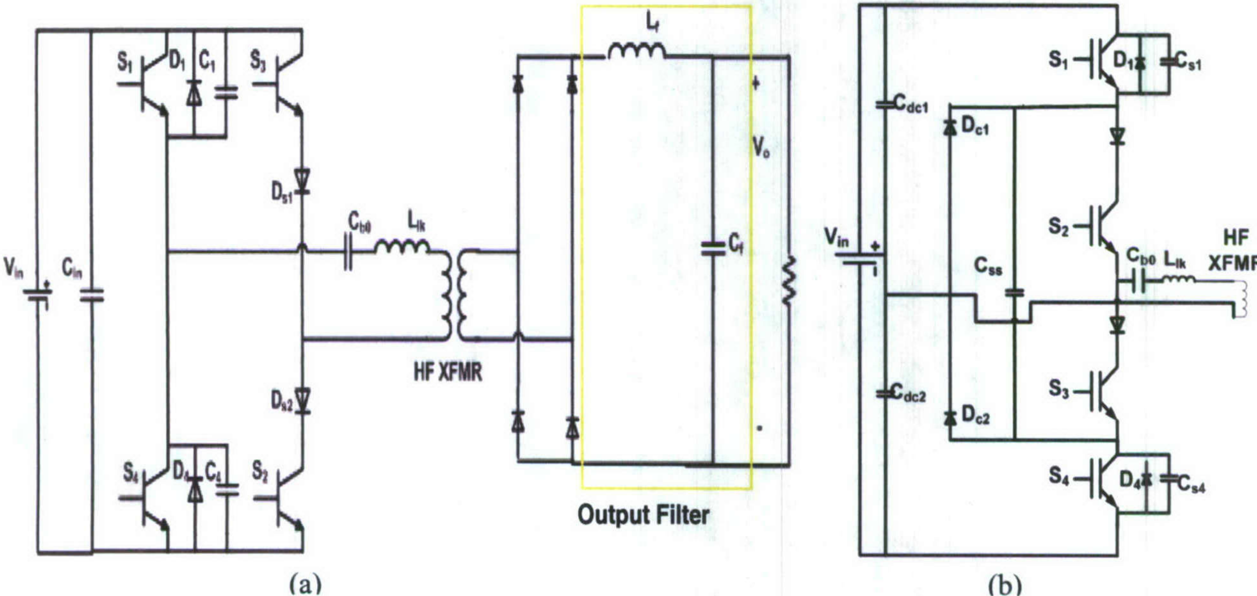

(a) (b)

Fig. 4.3 (a) Two-level ZVZCS converter, and (b) Three-level half-bridge ZVZCS converters [4.2].

Table 4.1: Bridge component parameters.

Parameter	Value
$V_{on,IGBT}$	1.5 V
$V_{on,diode}$	2 V
ESR_{Cb0}	0.005 Ω
ESR_{Lext}	0.026 Ω
I_{p0}	6.67 A
	200 ns
f_{sw}	10 kHz
C_r	6.8 nF
$C_{bo,2L}$	1.5 uF
$C_{b0,3L}$	6 uF
L_{lk}	10 uH

Fig. 4.5 summarizes the efficiencies for only the primary bridge of the converters. The HF-XFMR has poor efficiency (90%) reducing the overall system efficiency; future research work should be aimed at improving the transformer efficiency.

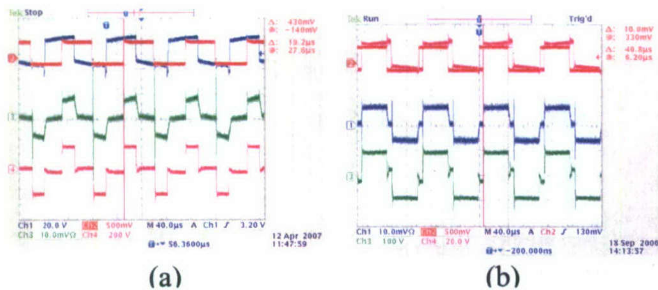

(a) (b)

Fig. 4.4 Waveforms at full load (10A):
(a) 2L FB: Ch.1 = v_{ge} S1 @ 20 V/div, Ch.2 = v_{ge} S2 @ 25 V/div, Ch.3 = I_p @ 10 A/div, Ch. 4 = v_{AB} @ 200 V/div
(b) 3L HB: Ch.1 = I_p @ 10 A/div, Ch.2 = v_{ge} S1 @ 25 V/div, Ch.3 = v_{AB} @ 100 V/div, Ch. 4 = v_{ge} S2 @ 20 V/div

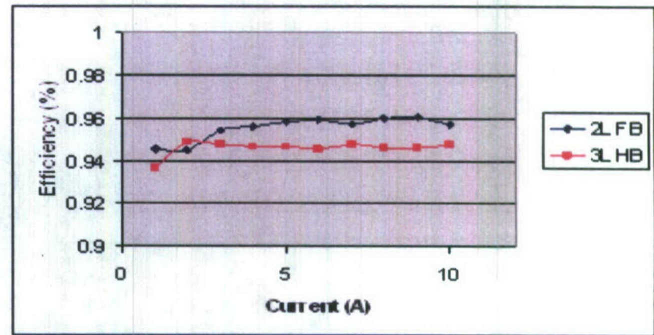

Fig. 4.5 Efficiency comparison for 2L FB converter and the 3L HB converter.

Conclusions

The main conclusions of this work were the following [4.2][4.3]:

- The three-level half-bridge converter uses switching devices with lower rated voltage, switching losses, conduction losses and cost. At higher switching frequencies, soft-switching converters should negate the increase in switching losses; so, the transformer size could be further reduced (by a lower step-down ratio and higher switching frequency) making this topology an attractive choice when volume becomes an overriding factor as it may be the case of an US Navy ship.
- From a design standpoint, the three-level half-bridge converter is a better choice if the converter does not require a large duty cycle range; that is, to operated over a wide load range.
- The two-level full-bridge converter has only a slightly larger soft-switching range β (that is, a range of $0.65° < \beta < 179°$ vs. $6° < \beta < 173°$ for the three-level half-bridge converter). Thus, it does not have a significant advantage when it comes to the electric load operating range.

Three-Level Full-Bridge ZVZCS Converters

This technical activity that built on the previous research effort evaluated a three-level full-bridge ZVZCS converter since twice the amount of power can be transferred from the primary to the secondary side [4.4]. Also, the number of PCM subsystems needed in Fig. 4.2 is reduced; this is important if the distribution voltage of an US Navy ship becomes 13.8 kV. A novel control algorithm was proposed as a result of this research work. Fig. 4.6 shows the considered electric topology which is derived from the three-level half-bridge topology of Fig. 4.3(b). Reference [4.4] provides a detailed description of the circuit design; once again, this information is not included in this report because of simplicity, ease of reading and space.

Experimental Results

A 200:48V, 480W prototype was designed, simulated in PSpice, and constructed to demonstrate the proposed converter. International Rectifier IRG4PC30KD IGBTs were used for the switching devices S_1-S_8, with HFA25TB60 HEXFRED diodes as the anti-parallel and series diodes D_1-D_8. Fast-switching On-Semi MUR1560 diodes were used for the clamping diodes D_{cl1}-D_{cl4}. In the prototype, Cree CSD10060A silicon carbide and IR 10ETF06 silicon Schottky diodes were used. The capacitors for the

dc bus, C_{dc}, were 2.2μF electrolytic, the clamping capacitors, C_{ss}, were 1μF polypropylene, and the parallel capacitors C_1, C_4, C_5, and C_8 were 4.7μF ceramic. The filter inductance and capacitance were selected to be large in order to emulate an ideal current source. The filter inductor was 1.7mH and the filter capacitor was 710μF.

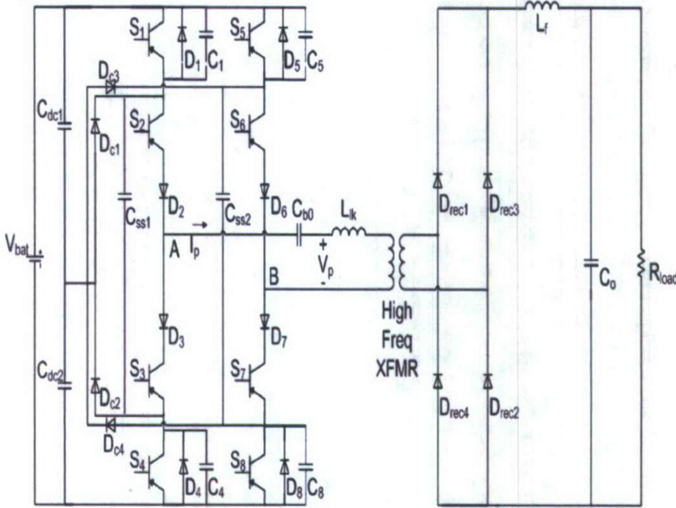

Fig. 4.6 Three-level full-bridge ZVZCS converter [4.4].

Figure 4.7 shows the experimental operational waveforms for both full load (10A) and light load (1A). Large spikes were seen in both the primary current and the primary voltage at the instant that the dc bus was applied to the transformer. Considering that a large change in voltage was applied to the system at this time, these spikes are not entirely unexpected. They come from the interaction of the series diode capacitance, C_{b0}, and the inductance of the transformer.

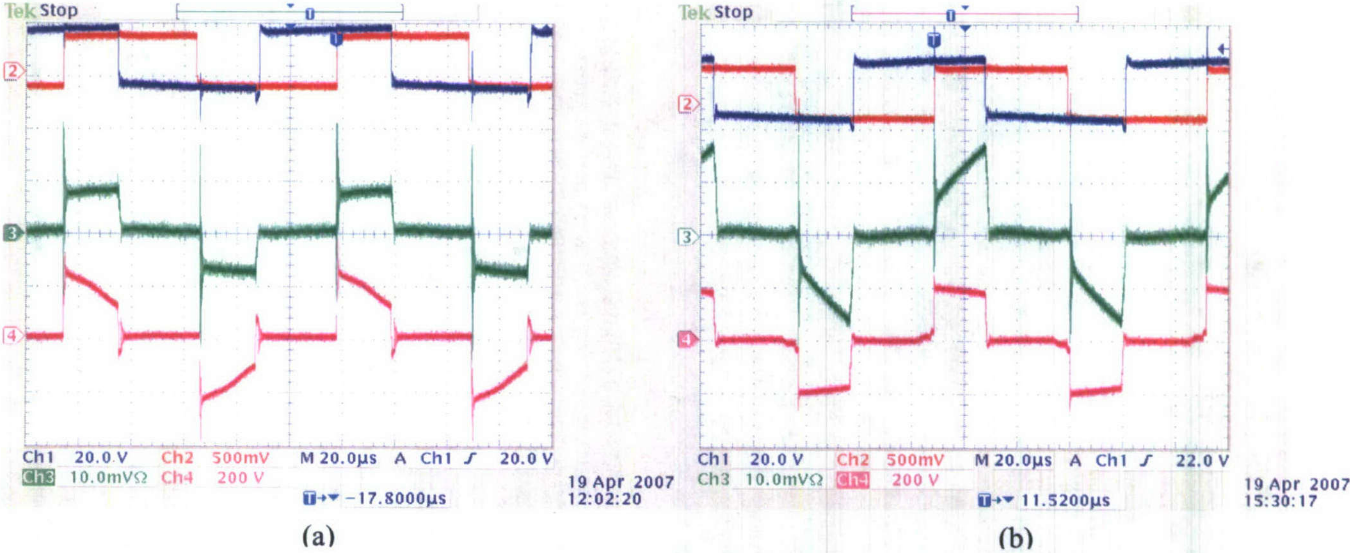

(a) (b)

Fig. 4.7 Operational waveforms for (a) full load (10A) and (b) light load (1A)
Ch. 1 = v_{ge} S_1 @ 20V/div; Ch. 2 = v_{ge} S_2 @ 25V/div; Ch. 3 = I_p @ 10A/div (a) or 1A/div (b); Ch. 4 = $v_{primary}$ @ 200V/div.

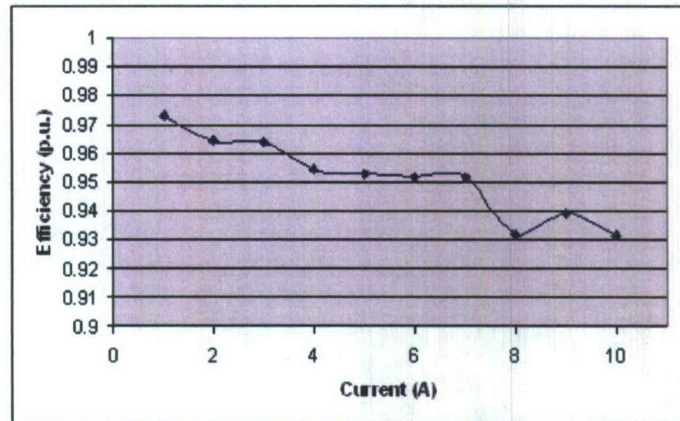

Fig. 4.8 Efficiency as a function of load current.

The spikes can reach twice the steady-state current and voltage, which should be kept in mind when selecting device ratings. The current ripple was the same for large or small currents, but it was not as evident in the full load condition since the scaling of the current is higher. Fig, 4.8 shows a plot of the efficiency as a function of the load current; efficiency drops off significantly as current increases due to the conduction losses in the series diodes D_2, $D_{3,}$, D_6, and D_7.

Conclusions

The main conclusions of this research work were that the proposed converter has the advantages of soft-switching and reduced voltage stresses across the devices, allowing higher voltage operation and thus making it suitable for PCM4 implementation [4.4].

Sub-task 4.2: A Novel Topology for Interfacing Multiple Non-Traditional Sources to an AC Power Grid

Introduction

Renewable energy sources (RES) are also considered by the US Navy under the "all-electric" ship concept due to reasons ranging from cost savings to tactical requirements [4.5]. Energy storage systems (ESS) are also evaluated for US Navy ships because of several reasons ranging from the energy required for advanced weaponry (e.g., the electromagnetic gun) to load leveling and ride-through capabilities during power interruptions [4.6][4.7]. The UA researchers anticipate that US Navy ships in the near term will continue to have an ac distribution (power) system at 4.16 kV and perhaps 13.8 kV as high-voltage power semiconductor devices become available with several non-traditional energy sources interfacing to the ac power grid. Non-traditional energy sources in the context of this report are fuel cells, photovoltaic and wind. Energy storage can be implemented by batteries, flywheels, superconducting magnetic storage, ultracapacitors and others. Therefore the main objective of this sub-task is to develop a novel topology for interfacing RES and battery-based energy storage to an ac power grid [4.8].

One form to integrate RES and energy storage is to connect them both to the ac power grid and transfer energy between them over the distribution lines [4.9]. The distribution line must be sized to handle the power flow from and to the RES. Therefore, methods which connect RES to energy storage locally are preferred when taking into account the reduced RES utilization because its power is not always available (e.g., wind is not blowing or PV arrays are not producing at night). Microgrids are one concept that integrates RES and energy storage as well as connecting them directly to the ac grid [4.10], allowing the complete system to be treated as a single unit by the ac grid. These systems are generally used to primarily provide power for a facility with local loads, and have their greatest benefit when optimized for such use; this could be the case of an US Navy ship having an electromagnetic gun.

Multiport converters share some similarities with microgrids in that they integrate several sources and energy storage on a common local bus, but they do not support for local loads. These converters use either a dc-bus [4.11] or a high-frequency ac bus [4.12]. Multiport converters using a dc bus often require that the bus voltage be stepped up, especially if they are using photovoltaic (PV) arrays as a supply, and electric isolation is sometimes a requirement. This creates a need for a transformer, either at line or high frequency, which is already accommodated in the case of using a HF ac bus. In addition to combining the boost and dc-HF-ac conversion functions into a single converter, a multiport converter with a HF transformer reduces the system size and weight compared to a system with a line frequency transformer. Furthermore, HF operation allows a reduction in the size of the other passive components in the system. The system described in [4.12] utilized a HF transformer with multiple taps on the primary side to integrate each non-traditional power sources and energy storage systems with the power grid. Additional sources can only be added if there are primary taps which are not used.

This report presents a novel topology which also uses a HF transformer (i.e., a HF ac bus), connecting non-traditional power sources and the ESS in parallel onto a *single* low-voltage primary side of the HF transformer [4.8]. The proposed topology is illustrated in Fig. 4.9 with switches *Z's* representing bi-directional switch assemblies for controlled bi-directional current flow. The high-voltage converter is connected to the power grid through a grid-interfacing inverter (represented by $V_{grid,dc}$ in Fig. 4.9), so power can flow either into or out of the grid. The top low-voltage converter is connected to a battery-based ESS, while the bottom low-voltage converter is connected to a RES; for example, a photovoltaic array. This design reduces the complexity of the transformer and it provides modular operation, allowing for the system to be expanded by adding additional RES and ESSs without having to replace the HF transformer (provided that it is properly sized to accommodate the additional converters). Furthermore each of the inputs can be controlled independently, so that each individual RES and ESS can operate under optimal utilization. Reference [4.7] provides information dealing with the design aspects which have been omitted in this report because of simplicity and space utilization.

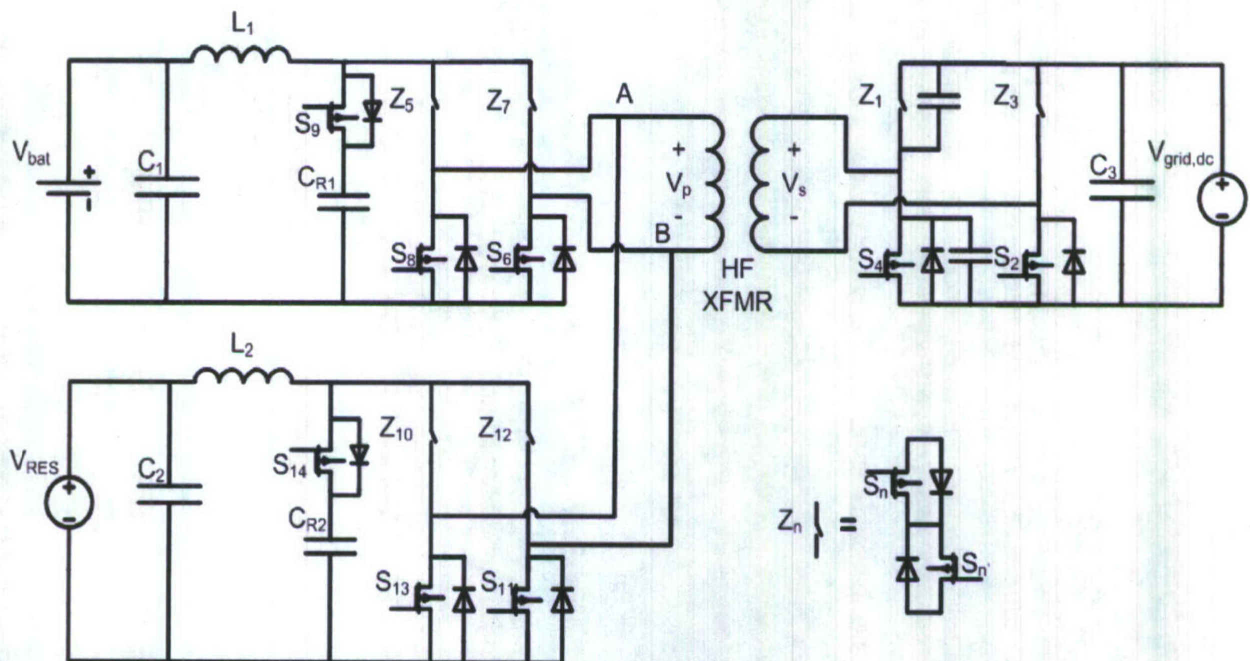

Fig. 4.9 Schematic of proposed system.

Power Flow and Operating Conditions
A general description of the operation of the system in Fig. 4.9 is as follows: The battery-based ESS sources or sinks whatever the difference is between the power produced by the RES and the power demanded or provided by the ship power grid, subject to the battery safe operating limits and stored energy. Thus, if the RES is providing more power than is needed by the power grid the ESS will be charged, whereas if the grid requires more power than the RES can provide the ESS will be discharged. If the RES is not providing any power, the power flow for the ESS will be equal to and opposite to the power flow on the power grid through the high-voltage converter.

Therefore, the operating conditions of the converter system in Fig. 4.9 can be defined in terms of the direction of power flow for each converter. Power can flow either into or out of the ESS, but power only flows out of the RES. Table 4.2 shows the seven operating conditions possible for the system given these definitions: "+" sign indicates that power flows out of that converter or that the converter is supplying power; "-" sign indicates that power flows into that converter or that the converter is consuming power; and "0" indicates that the converter is turned off for that particular operating condition. Thus, in operating condition I the RES is providing power to the ac grid and charging the ESS. In operating condition III, by contrast, both the RES and the ESS provide power to the ac grid.

Table 4.2 Operating Conditions.

Operating Condition	Converter		
	Grid	ESS	RES
I	-	-	+
II	-	0	+
III	-	+	+
IV	-	+	0
V	0	-	+
VI	+	-	+
VII	+	-	0

Determining the actual operating condition of the system depends on the status of the ac grid and on the state of charge of the battery-based ESS. The ac grid will usually have some sort of real and reactive power set points that will be determined by the ship controller optimizing the utilization of the ship's power producing resources (i.e., equivalent to a central dispatch in an electric utility system).

Experimental Results
A 15:200V, 20W prototype was designed and constructed to demonstrate the proposed converter. 300 V MOSFETs were used to implement the low voltage side devices, and the high voltage side was implemented with a rectifier since the high-side converter is acting like a rectifier for the operational mode under test. Two BK-Precision DC voltage supplies were used to simulate the battery and the RES, and a resistive load was put into place to emulate the grid. The upper converter in Fig. 4.9 consisting of switches Z_5, S_6, Z_7, and S_8 was run with a duty cycle of 0.6 and an input voltage of 20 V. The lower converter in Fig. 4.9 consisting of switches Z_{10}, S_{11}, Z_{12}, and S_{13} was run with a duty cycle of 0.4 and an input voltage of 14 V.

Fig. 4.10 shows the current on the secondary side of the transformer. Channels 1 and 2 show the gate signals for Z_5 and S_6, respectively, while channel 3 shows the voltage across the secondary side of the transformer. These channels have the same signals on Figs. 4.11-4.13 as well. Channel 4 on Fig. 4.10 shows the current on the secondary side of the transformer. This shows that power is flowing from the primary to the secondary. This current increases rapidly at first, but then settles into a constant value determined by the load resistance representing the ac grid. This is consistent with the behavior of an RL circuit, such as the one formed by the leakage inductance of the transformer and the resistance of the load (i.e., the resistance of the ac grid).

Fig. 4.11 shows the current through inductor L_1 in Fig. 4.9 on channel 4. This current is positive, showing that V_{bat} is contributing power to the ac grid. Fig. 4.12 shows the current through inductor L_2 on channel 4. This current is also positive, showing that V_{RES} is contributing power to the ac grid, but the average value of the current through L_2 is lower than the average value of the current through L_1, showing that V_{bat} is contributing more power to the ac grid than V_{RES} is. The amount of power that is contributed to the ac grid can be controlled by adjusting either the voltage magnitude at the input of each converter or by changing the duty cycle of each converter. The voltage V_{bat} has a larger voltage and a larger duty cycle than V_{RES}, so it contributes more power.

Figs. 4.13 and 4.14 show the currents through C_{r1} and C_{r2} respectively. These waveforms show that the capacitors are first charging and then discharging, and that the average current through them is zero. This is the expected behavior for these capacitors since they are meant to provide current balancing between L_1, L_2, and the ac grid. The sum of the two inductor currents and the two capacitor currents is equal to the current on the primary side of the transformer.

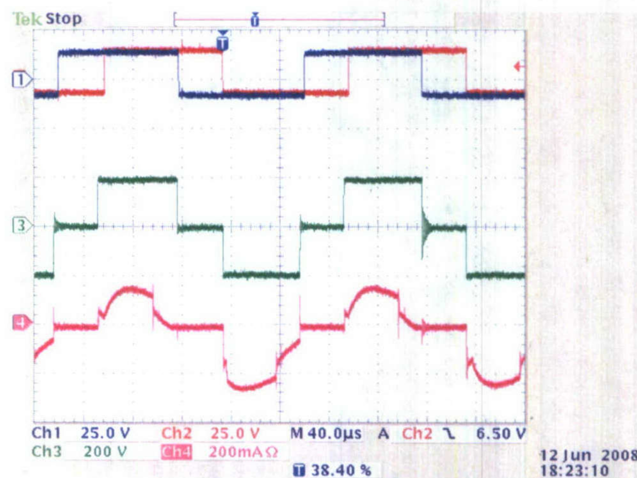

Fig. 4.10 Transformer high side voltage and current.
Channel 1: $V_{gs,Z5}$; Channel 2: $V_{gs,S6}$; Channel 3: $V_{XFMR,S}$; Channel 4: $I_{XFMR,S}$

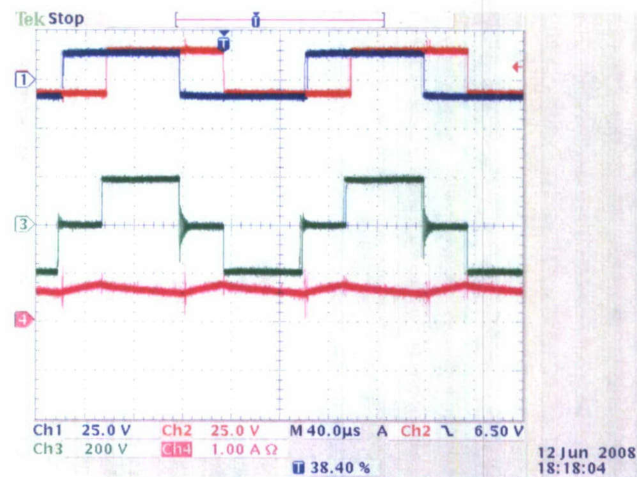

Fig. 4:11 Inductor L_1 current.
Channel 1: $V_{gs,Z5}$; Channel 2: $V_{gs,S6}$; Channel 3: $V_{XFMR,S}$; Channel 4: I_{L1}

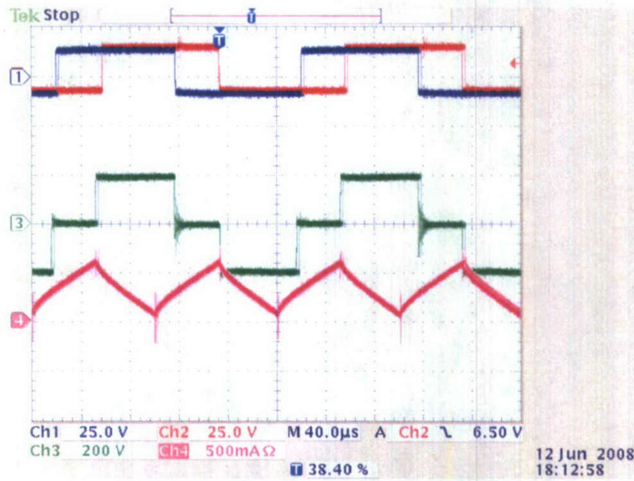

Fig. 4.12 Inductor L_2 Current

Channel 1: $V_{gs,Z5}$; Channel 2: $V_{gs,S6}$; Channel 3: $V_{XFMR,S}$; Channel 4: I_{L2}

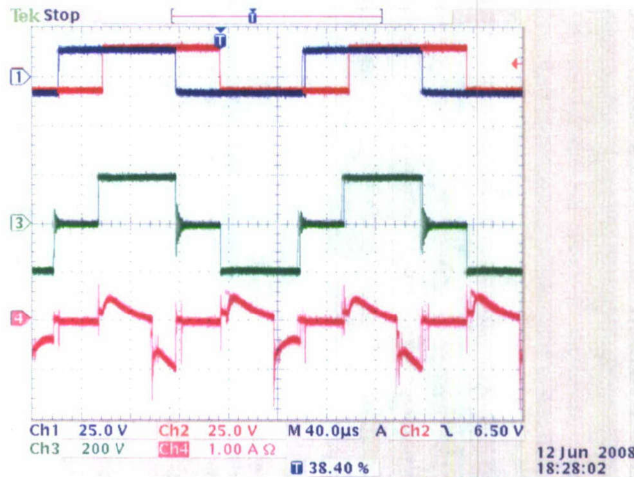

Fig. 4.13 Capacitor C_{r1} Current

Channel 1: $V_{gs,Z5}$; Channel 2: $V_{gs,S6}$; Channel 3: $V_{XFMR,S}$; Channel 4: I_{Cr1}

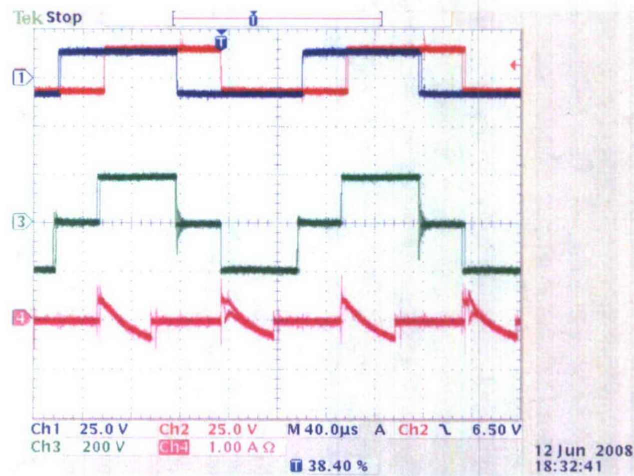

Fig. 4.14 Capacitor C_{r2} Current

Channel 1: $V_{gs,Z5}$; Channel 2: $V_{gs,S6}$; Channel 3: $V_{XFMR,S}$; Channel 4: I_{Cr2}

Conclusions

The proposed HF multiport converter system is a promising solution for the integration of distributed energy resources and energy storage onboard ships. The combination of the two using an integrated dc-dc converter can reduce losses over the ship distribution system and can allow for the RES to be treated as a source instead of a load variation, thus reducing the reliance on onboard traditional generators to provide fast acting power for energy-intensive weaponry systems, load leveling and other grid stability applications. More work is required to develop the full RES-ESS system.

References

[4.1] B. Reese, M. Schupbach, R. Saunders, B. Rowden, J. C. Balda, A. Lostetter, "High Voltage, High Power Density Bi-Directional Multi-Level Converters Utilizing Silicon and Silicon Carbide (SiC) Switches", *IEEE 2008 Applied Power Electronics Conference and Exposition*, Austin (TX), February 24-28, pp. 252-258.

[4.2] A. Medury, J. A. Carr, J. C. Balda, H. A. Mantooth, "An Evaluation of Two-Level and Three-Level Zero-Voltage and Zero-Current Switching Converters", *38th IEEE Power Electronics Specialists Conference PESC 2007*, Orlando (FL), June 17-22.

[4.3] A. Medury, J. A. Carr, J. C. Balda, H. A. Mantooth, T. Funaki, "Three-Level ZVZCS and ZVS Half-Bridge Converters: A Comparative Evaluation", *Power Conversion Conference – Nagoya 2007*, April 2-5, Nagoya, Japan, pp. 892-898.

[4.4] J. A. Carr, B. Rowden, J. C. Balda, "A Three-Level Full-Bridge Zero-Voltage Zero-Current Switching Converter With a Simplified Switching Scheme", *38th IEEE Power Electronics Specialists Conference PESC 2007*, Orlando (FL), June 17-22.

[4.5] J. S. Webster, H. Fireman, D. A. Allen, A. J. Mackenna and J. C. Hootman, "US Navy Studies on Alternative Fuel Sources and Power and Propulsion Methods for Surface Combatants and Amphibious Warfare Ships", *Naval Engineering Journal*, vol. 119, issue 2, 2007, pp. 35-48.

[4.6] H. Hegner, B. Desai, "Integrated Fight Through Power", *IEEE Power Engineering Society Summer Meeting*, vol. 1, 20-25 July 2002, pp. 336-339.

[4.7] J. V. Meer, A. Bendre, S Krstic, D. Divan, "Improved ship power system - generation, distribution, and fault control for electric propulsion and ship service", *IEEE 2005 Electric Ship Technologies Symposium*, 25-27 July 2005, pp. 284-291.

[4.8] J. A. Carr, J. C. Balda, "A Grid Interface for Distributed Energy Sources with Integrated Energy Storage Using a High Frequency AC Link", *IEEE 2008 Power Electronics Specialists Conference*, Rhodes, Greece, June 15-19.

[4.9] J.M. Carrasco et al, "Power-Electronic Systems for the Grid Integration of Renewable Energy Sources: A Survey," *IEEE Transactions on Industrial Electronics,* Vol. 53, Issue 4, June 2006, pp. 1002-1016.

[4.10] T.K. Panagrahi, S. Chowdhury, S.P. Chodhury, N. Chakraborty, Y.H. Song, "Control & Reliability Issue of Efficient Microgrid Operation Using Hybrid Distributed Energy Resources," *IEEE PES Power Systems Conference and Exposition*, October 29-November 1, 2006, pp. 797-802.

[4.11] Alexis Kwasinski, Philip T. Krein, "Multiple-input dc-dc converters to enhance local availability in grids using distributed generation resources," *Applied Power Electronics Conference*, February 2007, pp. 1657-1663.

[4.12] Rick West, "Bi-directional multi-port inverter with high frequency link transformer," U.S. Patent 7 102 251, September 5, 2006.

Task 5: Recommendations for Future Work

An analysis of the conclusions for each task or sub-task shows the following:

- The thermal management solution based on the jet-impingement methodology described in sub-task 2.3 has the potential of removing the heat fluxes typical of the power electronics forming the core of power conversion modules (PCM).
- The system packaging methodology for PCM described in sub-task 3.3 has the potential of achieving significant power densities at the system level.
- The PCM topologies described in task 4 have the potential of overcoming the system complexity issues typical of high-voltage PCM while achieving volume reductions and efficiency increases.

Therefore, the following research project is proposed to continue the above work:

Reliability Evaluation of Power Conversion Modules

A major issue with manufacturers of power electronics systems is reliability, in particular, as the power semiconductor device is subjected to heating/cooling cycles under normal operating conditions. Little work has been done in this area when it comes to SiC devices. There is a lot of interest from system integrators but besides cost none wants to be the first one to use devices whose reliability has not been proven. So there is a need for thermal testing under normal operating conditions.

One concern related to spray cooling (an active thermal management solution as opposed to passive ones like a simple heat sink) is the lack of thermal mass rendering a PCM non-operational in case of nozzle failure and thus affecting critical missions of the ship. The thermal solution in sub-task 2.3 overcomes the issue of nozzle failure and seems suitable for systems having high heat fluxes and large areas.

Wire bonds represent the main source of device failure; the proposed package in sub-task 3.1 has the potential of overcoming this disadvantage at the expense of complexity of the packaging process. The system packaging proposed in sub-task 3.3 when combined with the thermal solution of sub-task 2.3 have the potential of achieving important volume reductions.

Therefore, it is proposed a collaborative research project aimed at determining the reliability of SiC-based power conversion modules whose thermal management solution is the nozzle-less one described in sub-task 2.3 and packaging concept is the one in sub-task 3.3. This research project should involve the following participants:

- A manufacturer of electric ships (e.g., Northrop Grumman Newport News) to provide the specifications of the PCM,
- A manufacturer of SiC power devices (e.g., Cree Inc or Rohm-Japan),
- A manufacturer of PCM systems for the US Navy (e.g., SPCO or L3 Power Paragon)
- The UA research team.

From the specifications of the PCM (provided by the ship manufacturer), the manufacturer of PCM systems and UA researchers will design and construct a PCM prototype with the proposed thermal management solution (sub-task 2.3). The manufacturer of SiC power devices will provide the SiC devices. The SiC power devices will be packaged into power modules following the ideas in this report and subsequently tested for reliability. Envisioned tests for the power modules are the following: unsaturated pressure cooker, thermal cycling (TFT), thermal shock, and vibration. Finally, the developed PCM prototype will be tested according to the operational tests specified by the ship manufacturer.

A successful demonstration of the proposed ideas through this research project should shorten the adoption time of SiC device technology onboard ships since the ship manufacturer will be part of the project team and driving the specifications and performance metrics.

Publications Originated from this ONR-Sponsored Research

Task 2

R. P. Selvam, S. Sarkar, M. Sarkar and J. Johnston, "Modeling Multiphase Flow with Phase Change and Heat Transfer: Status Review, Challenges and Future Research Direction", accepted for a book chapter in Multiphase Flow Research, Nova Publication, 2008.

M. Sarkar, R.P. Selvam and R. Ponnappan, "Direct Simulation of Spray Cooling: Effect of multiple Droplet Impact and Latent Heat of Vaporization of Coolant Liquid on Heat Transfer", Proceedings of ASME Summer Heat Transfer Conference, Jacksonville, Florida, 2008, August 10-14.

R.P. Selvam, M. Sarkar, S. Sarkar, R. Ponnappan, and L.K. Yerkes, "Direct Simulation of Thermal Boundary Layer Effect on Liquid Vapor Interface Dynamics and Heat Transfer in Spray Cooling", paper submitted to *Journal of Thermophysics and Heat Transfer*, 2007.

R.P. Selvam, S. Sarkar and M. Sarkar, "Modeling Multiphase Flow and Heat Transfer – Current Status and Future Challenges", Invited paper for *7th Asian Computational Fluid Dynamics Conference*, IISC Bangalore, India, Nov. 26-30, 2007.

R.P. Selvam, M. Sarkar and R. Ponnappan, "Effect of Thermal Conductivity and Latent Heat of Vaporization of Liquid on Heat Transfer in Spray Cooling", Proceedings of *SAE*-Power *Systems Conference*, New Orleans, LA, USA, November 7-9, 2006.

R.P. Selvam, M. Sarkar, S. Sarkar and R. Ponnappan, "Effect of Vapor Bubble Size on Heat Transfer in Spray Cooling" Proceedings of *Space Technology and Applications International Forum (STAIF)*, AIP Conference on Thermophysics in Microgravity, Albuquerque, NM, 2006, Vol. 813, pp. 145-152.

R.P. Selvam, L. Lin and R. Ponnappan, "Direct Simulation of Spray Cooling: Effect of Vapor Bubble Growth and Liquid Droplet Impact on Heat Transfer", *Int. J. of Heat and Mass Transfer*, 2006, Vol. 49, pp. 4265-4278.

R.P. Selvam, M. Sarkar, and Ponnappan, R., "Modeling of Spray Cooling: Effect of Droplet Velocity and Liquid to Vapor Density Ratio on Heat Transfer", *16th Annual Thermal and Fluids Analysis Workshop (TFAWS)*, Univ. of Central Florida, Orlando, FL, 2005.

R.P. Selvam, S. Baskara, J.C. Balda, F. Barlow, and A. Elshabini, "Computer Modeling of Liquid Droplet Impact on Heat Transfer during Spray Cooling", Proceedings of *ASME Summer Heat Transfer Conference*, Paper # HT2005-72569, San Francisco, CA, 2005.

R.P. Selvam, L. Lin and R. Ponnappan, "Computational Modeling of Spray Cooling: Current Status and Future Challenges", *Space Technology and Applications International Forum (STAIF 2005)*, AIP conference proceeding on Thermophysics in Microgravity, Albuquerque, NM, 2005, Vol. 746, PP. 56-63.

R.P. Selvam and R. Ponnappan, "Numerical Modeling of Nucleation Boiling in Thin Film and Effect of Droplet Impact", 15th Annual Thermal & Fluid Analysis Workshop, Pasadena, CA, 2004.

Task 3

S.S. Ang, W.D. Brown, H. Mustain, B. Rowden, J.C. Balda, and A. Mantooth, "Packaging of Silicon Carbide Power Semiconductor Devices", *7th International Semiconductor Technology Ceonference-ISTC2008*, March 15-17, 2008, Shanghai, China.

K. Vanan, J. Junghans, F. Barlow, R. P. Selvam, J. C. Balda, A. Elshabini, "A Novel Packaging Methodology for Spray Cooling for Power Semiconductor Devices Using Dielectric Liquids", *IEEE 2005 Applied Power Electronics Conference (APEC'05)*, March 6-10, Austin (TX), Vol. 3, pp. 2014-2018.

Task 4

J. A. Carr, J. C. Balda, "A Grid Interface for Distributed Energy Sources with Integrated Energy Storage Using a High Frequency AC Link", *IEEE 2008 Power Electronics Specialists Conference*, Rhodes, Greece, June 15-19.

B. Reese, M. Schupbach, R. Saunders, B. Rowden, J. C. Balda, A. Lostetter, "High Voltage, High Power Density Bi-Directional Multi-Level Converters Utilizing Silicon and Silicon Carbide (SiC) Switches", *IEEE 2008 Applied Power Electronics Conference and Exposition*, Austin (TX), February 24-28, pp. 252-258.

J. A. Carr, D. Hotz, J. C. Balda, H. A. Mantooth, A. Ong, "Assessing the Impact of SiC MOSFETs on Converter Interfaces for Distributed Energy Resources", *42nd Annual Meeting of the IEEE Industry Applications Society*, New Orleans, September 23-27, 2007, New Orleans (LA).

A. Medury, J. A. Carr, J. C. Balda, H. A. Mantooth, "An Evaluation of Two-Level and Three-Level Zero-Voltage and Zero-Current Switching Converters", *38th IEEE Power Electronics Specialists Conference PESC 2007*, Orlando (FL), June 17-22.

J. A. Carr, B. Rowden, J. C. Balda, "A Three-Level Full-Bridge Zero-Voltage Zero-Current Switching Converter With a Simplified Switching Scheme", *38th IEEE Power Electronics Specialists Conference PESC 2007*, Orlando (FL), June 17-22.

A. Medury, J. A. Carr, J. C. Balda, H. A. Mantooth, T. Funaki, "Three-Level ZVZCS and ZVS Half-Bridge Converters: A Comparative Evaluation", *Power Conversion Conference – Nagoya 2007*, April 2-5, Nagoya, Japan, pp. 892-898.